Aus der Klinik für Allgemein-, Viszeral-, Tumor- und Transplantationschirurgie
der Universität zu Köln
Direktorin: Prof. Dr. med. Christiane Josephine Bruns

# Aldo-keto reductase 1C3 enhances radioresistance in esophageal adenocarcinoma via inhibiting ferroptosis

Inaugural-Dissertation zur Erlangung der Doktorwürde
der Medizinischen Fakultät
der Universität zu Köln

vorgelegt von
Feng Ju
Aus Jiangsu, China

promoviert am

Gedruckt mit Genehmigung der Medizinischen Fakultät der Universität zu Köln

Druckjahr

Dekan: Herr Univ.-Prof. Dr. Gereon R. Fink

1. Gutachterin oder Gutachter: Frau Univ.-Prof. Dr. Christiane J. Bruns
2. Gutachterin oder Gutachter:

Erklärung

Ich erkläre hiermit, dass ich die vorliegende Dissertationsschrift ohne unzulässige Hilfe Dritter und ohne Benutzung anderer als der angegebenen Hilfsmittel angefertigt habe; die aus fremden Quellen direkt oder indirekt übernommenen Gedanken sind als solche kenntlich gemacht.

Bei der Auswahl und Auswertung des Materials sowie bei der Herstellung des Manuskriptes habe ich keine Unterstützungsleistungen von folgenden Personen erhalten:

Prof. Dr. med. Christiane Josephine Bruns, Dr. Yue Zhao

Weitere Personen waren an der geistigen Herstellung der vorliegenden Arbeit nicht beteiligt. Insbesondere habe ich nicht die Hilfe einer Promotionsberaterin/eines Promotionsberaters in Anspruch genommen. Dritte haben von mir weder unmittelbar noch mittelbar geldwerte Leistungen für Arbeiten erhalten, die im Zusammenhang mit dem Inhalt der vorgelegten Dissertationsschrift stehen.

Die Dissertationsschrift wurde von mir bisher weder im Inland noch im Ausland in gleicher oder ähnlicher Form einer anderen Prüfungsbehörde vorgelegt.

Erklärung zur guten wissenschaftlichen Praxis:

Ich erkläre hiermit, dass ich die Ordnung zur Sicherung guter wissenschaftlicher Praxis und zum Umgang mit wissenschaftlichem Fehlverhalten (Amtliche Mitteilung der Universität zu Köln AM 132/2020) der Universität zu Köln gelesen habe und verpflichte mich hiermit, die dort genannten Vorgaben bei allen wissenschaftlichen Tätigkeiten zu beachten und umzusetzen.

Köln, den 11.09.2023 Unterschrift: .....

# Acknowledgements

Time flies, I still remember that I was a general surgeon three years ago, busy dealing with patients and performing surgeries every day in China, and now my doctoral studies are coming to an end in a blink of an eye in Germany. This is one of the most precious and unrepeatable experience in my life.

I am deeply indebted to the University of Cologne for this precious study opportunity. Furthermore, words cannot express my gratitude to my supervisors - Prof. Dr. Christiane J. Bruns and Dr. Yue Zhao, for their invaluable patience and great support. They are both outstanding scientists, and I could learn the courage to face difficulties and challenges from them.

I would like to express gratitude to our Surgical Lab group members: Ningbo Fan, Chenghui Zhou, Xiaolin Wu, Dr. Zhefang Wang, Susanne Neiß, Lisa Raatz, Michaela Heitman and Anke Wienand-Dorweiler, for their continuous help for my project. We are a group and more like a family; we care and support each other.

I am also thankful to: Prof. Margarete Odenthal and Xinlei Zhao for optimizing the Rstudio code of my sequencing data; Prof. Axel M. Hillmer and Dr. Sascha Hoppe for sharing the esophageal adenocarcinoma (EAC) cell lines and the experience of animal experiments; Jing Zhang for her support in the comet assay; Dr. Astrid Schauss and Beatrix Martiny for their support in the transmission electron microscopy imaging; Dr. Qu Jiang for optimizing the experimental protocols in flow cytometry and co-immunoprecipitation; Cologne Excellence Cluster for Cellular Stress Responses in Aging-Associated Diseases (CECAD) for the support in irradiation part; Prof. Thomas Langer and Dr. Soni Deshwal for their support of Seahorse experiments.

I would also like to thank my friend Dr. Stefan Pröbsting, I could not have undertaken this journey without his encouragement and help. Many thanks should also go to Dr. Wei Gao for his care and suggestion during my study.

I would like to extend my sincere thanks to Chinese Scholarship Council, for supporting on my study and life in Germany.

Last but not least, I want to thank my family - my grandparents and my parents. They gave me the utmost encouragement and support, allowing me to study in Germany with peace of mind.

Thanks to fate, let us meet in Germany in the past few years, and to everyone who has helped me, I would like to express my sincere thanks again!

# CONTENT


*CONTENT ..... 1*

*ABBREVIATION ..... 3*

*1. ZUSAMMENFASSUNG ..... 6*

*2. ABSTRACT ..... 7*

*3. INTRODUCTION ..... 9*

**3.1. Esophageal cancer ..... 9**

3.1.1. Introduction ..... 9

3.1.2. Management of EAC ..... 9

3.1.3. Radiotherapy resistance in EAC ..... 11

**3.2. Aldo-Keto-Reductase 1C3 and the potential role in regulation of radiotherapy response ..... 13**

3.2.1. Aldo-keto reductases family ..... 13

3.2.2. The role of AKR1C3 in radiotherapy ..... 15

**3.3. Ferroptosis ..... 16**

3.3.1. Introduction ..... 16

3.3.2. Ferroptosis in Cancer ..... 18

3.3.3. The role of ferroptosis in radiotherapy ..... 19

*4. AIM OF THE STUDY ..... 21*

*5. MATERIALS AND METHODS ..... 22*

**5.1. Materials ..... 22**

5.1.1. Cell lines ..... 22

5.1.2. Materials for cell culture ..... 22

5.1.3. Medium for cell culture and cryopreservation ..... 23

5.1.4. Materials for PCR ..... 23

5.1.5. Materials for protein analysis ..... 24

5.1.6. Materials for comet assay and electrophoresis ..... 26

5.1.7. Materials for plasmids construction and lentiviral transduction of mammalian cells 27

5.1.8. Materials for flow cytometry ..... 28

5.1.9. Materials for Co-immunoprecipitation (Co-IP) ..... 29

5.1.10. Materials for Seahorse experiments ..... 30

5.1.11. Chemicals and chemotherapy agents ..... 30

5.1.12. Laboratory equipments ..... 32

5.1.13. Consumable materials ..... 33

5.1.14. Software ..... 34

**5.2. Methods ..... 35**

5.2.1. Cell culture ..... 35

5.2.2. Cell counting ..... 35

5.2.3. Establishment of the radioresistant cell line ..... 36

5.2.4. Colony formation assay ..... 36

5.2.5. Immunofluorescence ..... 36

5.2.6. Quantitative Real-time PCR (qRT-PCR) ..... 37

5.2.7. Western blot ..... 37
5.2.8. Flow cytometry analysis ..... 37
5.2.9. Publicly available data analysis ..... 38
5.2.10. RNA sequencing and data analysis ..... 38
5.2.11. Statistical analysis ..... 38
*6. RESULTS ..... 39*
**6.1. Establishment and validation of the radioresistant EAC cell line model 39**
6.1.1. Establishment of the radioresistant EAC cell line model ..... 39
6.1.2. Validation of the radioresistant EAC cell line model *in vitro* ..... 39
**6.2. AKR1C3 could enhance the radioresistance in EAC cells ..... 41**
6.2.1. AKR1C3 improves colonies survival fraction after irradiation ..... 41
6.2.2. AKR1C3 regulates the irradiation-induced apoptosis in EAC cells ..... 42
**6.3. AKR1C3 reduces the DNA damage after irradiation in EAC cells ..... 43**
**6.4. AKR1C3 influences the mitochondrial function in EAC cells ..... 45**
6.4.1. Mitochondrial morphology alters in the radioresistant model ..... 45
6.4.2. AKR1C3 regulates mitochondrial metabolism in EAC cells ..... 45
6.4.3. AKR1C3 regulates mitochondrial activity after radiotherapy in EAC cells ..... 45
**6.5. AKR1C3 inhibits irradiation-induced ferroptosis in EAC cells ..... 47**
6.5.1. AKR1C3 is closely related to ferroptosis ..... 47
6.5.2. AKR1C3 suppresses erastin-induced ferroptosis in EAC cells ..... 49
6.5.3. AKR1C3 inhibits the irradiation-induced ferroptosis in EAC cells ..... 50
**6.6. AKR1C3 inhibitor could re-sensitize EAC cells to erastin. ..... 51**
6.6.1. Ferrostatin-1 (Ferr-1) could cause the radioresistance in AKR1C3 knockdown cells. 51
6.6.2. AKR1C3 inhibitor could re-sensitize EAC cells to erastin ..... 52
**6.7. AKR1C3 mRNA expression level was upregulated in esophageal cancer and related to poor prognosis ..... 54**
*7. DISCUSSION ..... 55*
*8. REFERENCE ..... 60*

## ABBREVIATION

AIFM2: Apoptosis-inducing factor mitochondrial 2
AKRs: Aldo-keto reductases
AKR1: Human aldo-keto reductase family 1
AKR1C1: Human aldo-keto reductase family 1 member C1
AKR1C2: Human aldo-keto reductase family 1 member C2
AKR1C3: Human aldo-keto reductase family 1 member C3
AKR1C4: Human aldo-keto reductase family 1 member C4
AKT: Protein kinase B
BE: Barrett's esophagus
BRCC3: BRCA1-BRCA2-containing complex 3
ChIP: Chromatin immunoprecipitation
CI: Confidence interval
Co-IP: Co-immunoprecipitation
CoQ: Coenzyme Q10
$CoQH_2$: Reduced coenzyme Q10
CROSS: ChemoRadiotherapy for Oesophageal cancer followed by Surgery Study
CRT: Chemoradiotherapy
CSCs: Cancer stem cells
DAPI: 4 ', 6-diamidino-2-phenylindole, dihydrochloride
DAU: Daunorubicin
DEGs: Differentially expressed genes
DHT: Dihydrotestosterone
DHODH: Dihydroorotate dehydrogenase
DMSO: Dimethyl sulfoxide
DNA: Deoxyribonucleic acid
DSBs: DNA double strands breaks
DOX: Doxorubicin
EAC: Esophageal adenocarcinoma
EC: Esophageal cancer
ECAR: Extracellular acidification rate
EDTA: Ethylenediaminetetraacetic acid
EGFR: Epidermal growth factor receptor
EMR: Endoscopic mucosal resection
EMT: Epithelial-mesenchymal transition
ER: Endoplasmic reticulum
ESD: Endoscopic submucosal dissection
ESCC: Esophageal squamous cancer cells
ESMO: European Society for Medical Oncology
FBS: Fetal bovine serum
FINs: Ferroptosis inducers
FSP1: Ferroptosis inhibitor protein 1
GEO: Gene Expression Omnibus
GEPIA: Gene Expression Profiling Interactive Analysis
GERD: Gastroesophageal acid reflux disease
GPX4: Glutathione peroxidase 4

GSEA: Gene set enrichment analysis
GSH: Glutathione
GSSG: Glutathione disulfide
HCC: Hepatocellular carcinoma
HNSCC: Head and neck squamous cell carcinoma
$H_2O_2$: Hydrogen Peroxide
HUGO: Human genome project
HR: Hazard Ratio
IL6: Interleukin 6
IR: Ionizing Radiation
KEAP1: Kelch-like ECH associated protein 1
KRAS gene: Ki-ras2 Kirsten rat sarcoma viral oncogene homolog
L-OH: Phospholipid alcohols
L-OOH: Phospholipid hydroperoxides
MAPK: Mitogen-activated protein kinases
OCR: Oxygen consumption rate
PCR: Polymerase chain reaction
PDAC: Pancreatic ductal adenocarcinoma
PG: Prostaglandin
$PGD_2$: Prostaglandins $D_2$
$PGF_2$: Prostaglandin $F_2$
$PGF_{2\alpha}$: Prostaglandins $F_{2\alpha}$
$PGH_2$: Prostaglandins $H_2$
PI3K: Phosphoinositide 3-kinase
NADPH: nicotinamide adenine dinucleotide phosphate
NF-κB: Nuclear factor kappa B
NRF2: Nuclear factor erythroid 2-related factor 2
NSCLC: Non-small-cell lung cancer
MFI: Median fluorescence intensity
MPA: Medroxyprogesterone acetate
MPTP: Mitochondrial permeability transition pore
MTT: 3-(4, 5-dimethyl-2-thiazolyl)-2, 5-diphenyl-2-H-tetrazolium bromide
O2▪−: Superoxide
OH▪: Hydroxyl radical
OPSCC: Oropharyngeal squamous cell carcinoma
OS: Overall survival
PBS: Phosphate buffered saline
qRT-PCR: Quantitative Reverse Transcription PCR
RBMS1: RNA-binding motif, single-stranded-interacting protein 1
RCC: Renal cell carcinoma
RNA: Ribonucleic acid
ROS: Reactive oxygen species
RPA3: Replication protein A 3
RSL3: RAS-selective lethal 3
RT: Radiation therapy
RT-PCR: Reverse transcription polymerase chain reaction
SDS: Sodium dodecyl sulfate
shRNA: short hairpin RNA

SCD1: Stearoyl-CoA desaturase 1
SLC3A2: Solute Carrier Family 3 Member 2
SLC7A11: Solute Carrier Family 7 Member 11
SNAIL1: snail family transcriptional repressor 1
SPIONCs: Self-assembled pH-sensitive superparamagnetic iron oxide nanoclusters
STAT3: Signal transducer and activator of transcription 3
STC2: Stanniocalcin 2
TCGA: The Cancer Genome Atlas
TIM: Triosephosphate isomerase
TME: Tumors microenvironment
TMRE: Tetramethyl rhodamine ethyl ester
VDAC2/3: Voltage-dependent anion channel 2/3
xCT: Cystine transporter

# 1. ZUSAMMENFASSUNG

Das Ösophagus-Karzinom (EC) besitzt die sechsthöchste Sterblichkeitsrate und siebthöchste Inzidenz weltweit. In Ländern mit hohem Einkommen ist das Adenokarzinom des Ösophagus (EAC) der häufigste Subtyp. Trotz der bemerkenswerten Verbesserungen in der Diagnose und der Behandlung in den letzten Jahrzehnten liegt die 5-Jahres-Gesamtüberlebensrate von EAC-Patienten weltweit immer noch unter 15 Prozent.

Die Strahlentherapie, als traditionelle adjuvante Therapie, hat in den letzten Jahrzehnten die Prognose der Patienten verbessert. Allerdings bleibt die Resistenz gegen solch eine Therapie ein enormes Hindernis für die Verbesserung der therapeutischen Wirksamkeit. AKR1C3 stellt ein vielversprechendes therapeutisches Ziel zur Überwindung der Strahlenresistenz bei vielen Krebsarten dar, während der molekulare Mechanismus von AKR1C3 bezogen auf die Strahlenresistenz in EAC-Patienten noch unklar ist. Um den Mechanismus der Strahlenresistenz in EAC zu untersuchen, haben wir zunächst ein *in vitro* Modell zur Untersuchung der Strahlenresistenz in EAC etabliert. RNA-Sequenzanalysen und Western Blot Untersuchungen bestätigten, dass AKR1C3 in OE33R (der strahlenresistenten EAC-Zelllinie) im Vergleich zu OE33P (der parentalen EAC-Zelllinie) hochreguliert war. Basierend auf den transkriptomischen Daten stellten wir fest, dass der Ferroptoseweg in der KEGG-Analyse angereichert war.

Anschließend haben wir bestätigt, dass AKR1C3 die Strahlenresistenz in unseren AKR1C3-überexprimierenden und Knockdown-EAC-Zelllinien erhöhen kann. Die Überexpression von AKR1C3 führte zu einer Verringerung der DNA-Schädigung, während die Unterdrückung von AKR1C3 zu einer erhöhten Schädigung führte. Darüber hinaus könnte eine Überexpression von AKR1C3 die mitochondriale Aktivität nach der Bestrahlung steigern, während ein Abbau von AKR1C3 diese schwächte. Wichtig ist, dass das AKR1C3-Expressionsniveau durch die GEPIA-Korrelationsanalyse positiv mit SLC7A11 und GPX4 korrelierte. Die Überexpression von AKR1C3 führte zu einer verringerten Lipidperoxidation, während eine Hemmung von AKR1C3 EAC-Zellen erneut für die Ferroptose sensibilisieren könnte.

Abschließend lässt sich sagen, dass wir zum ersten Mal berichten konnten, dass AKR1C3 die Strahlenresistenz durch Hemmung der Ferroptose in EAC-Zellen in erhöhen könnte. Die gezielte Behandlung von AKR1C3 könnte einen neuartigen Ansatz zur Überwindung der Strahlenresistenz bei EAC-Patienten darstellen.

# 2. ABSTRACT

**Background:**

Esophageal cancer (EC) is the 6$^{th}$ highest mortality and 7$^{th}$ highest incidence worldwide. Overall, esophageal adenocarcinoma (EAC) is the most common subtype of EC in high-income countries. Aldo-keto reductase 1C 3 (AKR1C3) represents a promising therapeutic target to overcome radioresistance in many cancers, while the molecular mechanism of AKR1C3 in the radioresistance of EAC is still unclear.

**Methods:**

The radioresistant model of OE33 was established by long-term small-dose irradiation (IR). Colony formations were performed to validate the survival fraction of EAC cells. RNA-seq analysis was applied for the *in vitro* radioresistant model. AKR1C3 overexpressing cells (generated from OE33) and knockdown cells (modified from SKGT-4) were established for *in vitro* analysis. The IR-induced apoptosis levels were measured by flow cytometry with DAPI and Annexin V staining. DNA damage levels were measured by immunofluorescence with gamma-H2AX staining and by Comet assay. The mitochondrial morphology of EAC cells was photographed by transmission electron microscope. Seahorse XF cell mito stress tests and Seahorse XF glycolytic rate assays were performed to measure oxygen consumption rate (OCR) and extracellular acidification rate (ECAR), respectively. Tetramethyl rhodamine ethyl ester (TMRE) staining was used for measuring mitochondrial activities. SLC7A11 and GPX4 protein levels were measured by Western blot. Lipid peroxidation levels were measured by flow cytometry with C11-Bodipy staining. MTT assays were applied to measure cell viability after erastin-treatment in EAC cells. Furthermore, Kaplan-Meier survival analysis was performed to draw the survival curve from the TCGA survival data.

**Results:**

Colony formation assay validated the radioresistant model of EAC cell line. The RNA-seq analysis showed a higher mRNA level of AKR1C3, as well as some ferroptosis-related genes such as FSP1 and SLC7A11 in the radioresistant cell line than in the parental cell line. Western blot and qRT-PCR confirmed the expression of AKR1C3 in our radioresistant model. In addition, overexpression of AKR1C3 in EAC cells significantly improved the survival fraction and decreased the apoptotic cells after irradiation. Overexpression of AKR1C3 could also prevent EAC cells from DNA damage after irradiation. The reversed results were observed in AKR1C3 knockdown cells.

Transmission electron microscope exhibited mitochondrial morphological changes after irradiation in EAC cells. AKR1C3 overexpressing cells showed more oxygen consumption rate changes after irradiation than the control cells. Higher TMRE levels were observed in AKR1C3 overexpressing cells after irradiation, while TMRE levels were lower in AKR1C3 knockdown cells. SLC7A11 and GPX4 expression levels showed a positive correlation with AKR1C3 by Western blot and GEPIA database analysis. Overexpression of AKR1C3 exhibited more resistant to erastin treatment, while knockdown of AKR1C3 sensitized cells to erastin treatment. Lipid peroxidation levels were lower in AKR1C3 overexpression cells and radioresistant cells while higher in AKR1C3 knockdown cells after irradiation or erastin treatment. MPA, a selective AKR1C3 inhibitor, could re-sensitize EAC cells to erastin treatment. The survival curve showed the median survival time was 23.1 months in the high AKR1C3 group and 27.1 months in the low AKR1C3 group in EAC cohort.

**Conclusions:**

In this study, we demonstrated AKR1C3 could regulate the radioresistance of EAC cells. AKR1C3 renders radioresistance through inhibition of ferroptosis via mediating SLC7A11/GSH/GPX4 axis. Targeting AKR1C3 may provide a potential approach to increase the treatment response in EAC patients for individualized therapy.

**Key words:** esophageal adenocarcinoma; Aldo-keto reductase 1C 3 (AKR1C3); radioresistance; ferroptosis; lipid peroxidation

# 3. INTRODUCTION

## 3.1. Esophageal cancer

### 3.1.1. Introduction

Esophageal cancer (EC) is the 6th highest mortality (544,000 deaths in 2020) and 7th highest incidence (604,000 new cases in 2020) worldwide, which accounts for an estimated 1 in every 18 cancer deaths [1]. The incidence is lower in Western countries than in Eastern Asia and Southern Africa [2].

Esophageal squamous cell carcinoma (ESCC) and Esophageal adenocarcinoma (EAC) are the two major subtypes of esophageal cancer by histology, while small-cell carcinoma, melanoma, sarcoma, and lymphoma are relatively rare [3]. Overall, ESCC is the most common subtype of EC, while EAC represents approximately two-thirds of total EC cases in high-income countries [1]. ESCC and EAC differ in etiology and pathogenesis, molecular biology, locations in the esophagus and therapeutic sensitivity but are similar in prognosis [2].

Mechanically, ESCC is mainly associated with cigarette and alcohol consumption [4], and use of both could increase an approximately threefold risk for ESCC [5]. Compared to EAC, ESCC is highly associated with the most socially deprived quintile and is more common in economically deprived groups and regions [6]. However, EAC doesn't present this trend. EAC is associated with excess body weight, gastroesophageal reflux disease and Barrett's esophagus [7]. The incidence of EAC is expected to rise rapidly among high-income countries and has already or will surpass the incidence of ESCC in the next few years [8].

EAC is the predominant histological type in Europe, such as Germany and other Western countries, while ESCC is the major subtype in Eastern Asia, especially in China and Japan [9]. Despite the remarkable improvements in diagnosis and treatment in the past decades, the overall 5-year survival of EAC patients is still lower than 15% worldwide [10]. Most cases are diagnosed in an advanced stage or even with metastasis when the prognosis is dismal. Thus, there is an urgent need for effective screening and multi-disciplinary management strategies to improve the overall prognosis.

### 3.1.2. Management of EAC

Although ESCC is the major subtype worldwide, in Western Europe and the United States, EAC is a more prevalent histological type that has been validated to be associated with obesity, gastroesophageal acid reflux disease (GERD) and Barrett's

esophagus (BE) [7,11]. GERD affects approximately 15% to 20% of the Western population, but only 10% to 15% of these patients have BE [12]. Although BE is clearly a precursor, only 0.12% to 0.60% of the BE patients develop to EAC each year [13]. Nowadays, most patients with GERD are undergoing regular upper endoscopy and surveillance for Barrett's esophagus, while only less than 15% of EAC cases are successfully screened during BE surveillance [14,15]. Only few EAC patients are diagnosed as a localized disease at the time of presentation, severely impeding effective treatment approaches [13].

Barium esophagrams is a classic screening method for upper gastrointestinal tumors, which can identify irregular lesions, but the screening accuracy is not enough, and it has been abandoned in many regions [16]. Upper endoscopy combined with biopsy histologic detection is the gold standard for the diagnosis of upper gastrointestinal tumors. However, the high cost and severe discomfort prevent endoscopy from being used for widespread screening. Computed tomography is an examination method with high acceptance by patients, but similar to endoscopy, its high examination cost is a disadvantage. A recent study showed screening every two years in the high-risk area would be the most cost-effective strategy, and the initial screening age is 40 to 44, which is mostly associated with health benefits [17]. According to the different morbidity, economic status and medical conditions in different regions, choosing the appropriate screening to maximize the benefits would be an optimal strategy.

Treatment strategies for EAC depend on several crucial factors, including tumor size and location, tumor stage, underlying health condition, age, and the patient's personal expectations. Given the fact that systemic treatment usually cannot cure EAC, surgical or endoscopic approaches should be actively performed for patients with early-stage [18]. For advanced patients, multidisciplinary treatment, including chemotherapy, radiotherapy and immunotherapy, have become the consensus among gastroenterology oncologists [19].

Decisions made for the initial treatment of EC are based on clinical staging, which should include the complete blood tests and clinical examination, endoscopic diagnosis and computed tomography. Endoscopic ultrasound is recommended to perform for the accurate assessment of T / N stage in potentially resectable esophageal tumors by ESMO Clinical Practice Guideline [20]. Endoscopic mucosal resection (EMR) and endoscopic submucosal dissection (ESD) are the two major endoscopic resection methods for patients with esophageal cancer [21]. Both of them provide the accurate information of the invasion depth according to the pathological diagnosis. To reach the complete resection, multiple endoscopic resections could be performed [18].

Given the enormous surgical trauma and potential postoperative complications, esophagectomy is generally not the first choice for treating superficial tumors. However,

esophagectomy is often an alternative for superficial tumors after ESD or EMR failure [13,22]. Clinical trials revealed neoadjuvant chemoradiotherapy followed by surgery could improve overall survival than surgery alone in patients with esophageal cancer [23-25]. Minimally invasive esophagectomy is the trend of surgical development in recent years, which relies on the rapid development of thoracoscopy, laparoscopy or robot technology [26].

ChemoRadiotherapy for Oesophageal cancer followed by Surgery Study (CROSS) comparing neoadjuvant chemoradiotherapy plus surgery versus surgery alone in patients with EAC and ESCC showed a significant survival benefit in 5-year overall survival for the neoadjuvant chemoradiotherapy with surgery group [27]. The result of this trial showed: in patients with EAC group, median overall survival was 43.2 months (95% CI 24.9-61.4) in the neoadjuvant chemoradiotherapy followed by surgery group and 27.1 months (95% CI 13.0-41.2) in the surgery alone group (HR 0.73 [95% CI 0.55-0.98]; log-rank p=0.038). Nowadays, based on a large number of clinical trials and prognostic analysis, preoperative neoadjuvant chemoradiotherapy has become the expert consensus for advanced EAC as well as ESCC [20,28-31].

The popularity of biomarker detection technology has improved the accuracy of EC diagnosis and targeted therapy. Compared with traditional tissue biopsy, liquid biopsy has been increasingly studied and optimized as a minimally invasive diagnostic tool. Cell-free DNA (cfDNA) has been proven to be an effective circulating biomarker, which can be used in cancer diagnosis and provide a reference for comprehensive treatment of cancers [32]. Furthermore, target therapy on HER2 and PD-L1 also showed good efficacy in EC [33]. In the future, targeted therapy based on genetic testing may become a routine approach as a supplement to traditional anti-tumor therapy.

### 3.1.3. Radiotherapy resistance in EAC

EAC is relatively more radioresistant than ESCC, all the patients who are resectable with local EAC which is potentially curable should be considered for neoadjuvant treatment after surgery [34]. The overall survival of esophageal cancer has benefited from the development of new agents and the popularity of chemoradiotherapy in the past few decades, but the overall 5-year survival rate is still dismal [1,35]. The main causes of the low survival are tumor recurrence and metastasis due to the therapy resistance [36]. Therapy resistance is a complicated and heterogeneous clinical feature, involving multiple molecular and pathophysiological mechanisms (Fig 3.1.3) such as DNA damage and repair, physical barriers, tumor microenvironment, gene mutations, epigenetic alterations and tumor heterogeneity [37,38]. The FLOT regimen, including fluorouracil, leucovorin, oxaliplatin, and docetaxel, is recognized as a standard perioperative

chemotherapy regimen [39]. However, an increasing number of patients are found to be chemo-resistant. Our previous study revealed AKR1C3 could enhance chemoresistance via AKT / GSH axis [40].

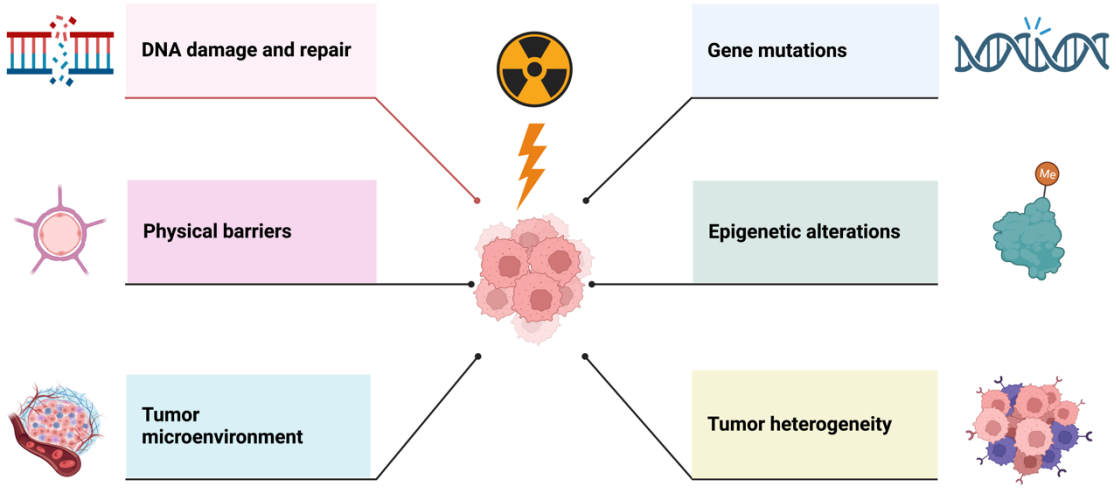


**Fig 3.1.3 The molecular and pathophysiological mechanisms of radioresistance**
The main molecular and pathophysiological mechanisms of radioresistance were exhibited in the figure, such as DNA damage & repair and tumor heterogeneity.

Radiation therapy (RT) is one of the most effective approaches of cytotoxic treatment based on ionizing radiation (IR) [41]. The key points to radiotherapy for EAC patients are to improve the accuracy of localization, reduce the damage to the surrounding tissues and assess the dose for individual patients. Despite continuous advances in the technology of radiotherapists, radioresistance remains an enormous obstacle to increasing RT efficacy [42]. With the deepening of molecular mechanism research, radioresistance has been gradually revealed in recent years. BRCC3, a novel multiprotein participating in the DNA damage response, is associated with poor survival in pretreatment patients of nasopharyngeal carcinoma [43]. The expression level of DNA damage repair marker RPA3 in the post-treatment sample was higher in radioresistant nasopharyngeal carcinoma patients who had local recurrence, and it is associated with the poor overall survival in patients of head and neck squamous cell carcinoma (HNSCC) with RT [44]. The radioresistant EAC cells presented a stronger repair capacity of IR-induced DNA damage [45], suggesting radioresistance is associated with the DNA damage repair mechanism in EAC. Besides DNA damage repair, radioresistance in EAC has also been reported to be related to other mechanisms, such as hypoxia. Elodie et al. [46] found irradiation was less effective in hypoxic tumors (tumor-to-background (T/B) ratios ≥ 3.59) compared to normoxic tumors (T/B < 3.59); in vitro, cells pre-treated with nimorazole

significantly decreased hypoxic radioresistance ($P < 0.01$), while in vivo, cancer cell proliferation was inhibited by the enhanced efficacy of RT, which was induced by nimorazole. Non-coding RNAs (miRNA and lncRNA), immunomodulation and cancer stemness have also been reported to be closely related to radioresistance in EAC [47-50]. Further exploration of the molecular mechanism underlying radioresistance in EAC might be helpful in assessing treatment efficiency and improving prognosis in patients with radioresistant EAC.

## 3.2. Aldo-Keto-Reductase 1C3 and the potential role in regulation of radiotherapy response

### 3.2.1. Aldo-keto reductases family

Aldo-keto reductases (AKRs), a superfamily of NAD(P)(H)-dependent oxidoreductases, are predominantly found in the cytoplasm of nearly all phyla, usually as monomers with a molecular weight of 34-37 kDa [51]. The AKRs protein superfamily contains 190 annotated proteins grouped into 16 families [52]. In living organisms, their main function is to catalyze the reduction of carbonyls to alcohols. Aldehydes are reduced to primary alcohols and ketones are reduced to secondary alcohols through the action of AKRs [53]. Each enzyme has the similar protein fold, a triose-phosphate isomerase TIM barrel or (α/β)8-barrel inserted with several additional helices [54]. There are three large loops at the back of the barrel, which help define substrate specificity and recruit different amino acids into the binding pocket based on the substrate [51]. AKR families and subfamilies are identified by sequence alignment, where associated members are grouped according to protein function [55].

The AKR1C family genes are comprised of 12 exons and located on chromosome 10 p15-p14 [56]. These enzymes have an 84-98% similar of amino-acid sequence identity, especially AKR1C1 and AKR1C2, with 97% sequence homology and only seven amino-acid residues are different [57]. In the AKR1 subfamily, AKR1C1 (20α(3α)-HSD, DD1), AKR1C2 (Type 3, 3α-HSD, DD2), AKR1C3 (Type 2, 3α-HSD, Type 5 17β-HSD, DDX) and AKR1C4 (Type 1, 3α-HSD, DD4) are recognized by the human genome project (HUGO).

AKR1C1 is involved in the synthesis and metabolism of numerous crucial substances in the body, including steroids, prostaglandins, fats, hormones, glucocorticoids and polycyclic aromatic hydrocarbons [58]. Given the fact that critical physiological functions and widespread expression in tissues, AKR1C1 has been reported to exist in large expression differences between tumor and normal tissue, for instance, non-small cell

lung cancer, cervical cancer, ovarian cancer, breast cancer, endometrial cancer and head and neck squamous cell carcinoma [59-66]. As a reductase involved in various carbonyl reduction reactions, AKR1C1 has also been reported to be involved in the metabolism of various drugs [67-69]. Through years of molecular biology and pharmacological studies, AKR1C1 is mainly related to gynecological diseases, which may be related to its regulation of hormone levels.

The main function of AKR1C2 is to reduce dihydrotestosterone (DHT) to 3α-diol [70]. Qing et al. [71] found that selective loss of AKR1C2 in prostate cancer cells could promote cell growth by enhancement of androgen-dependent cellular proliferation by regulating DHT metabolism. Recent bioinformatic studies revealed AKR1C2 was correlated with a positive prognosis in thyroid carcinoma and could activate the PI3K/AKT signaling pathway in ESCC, suggesting AKR1C2 is a potential biomarker with prognostic value in these types of cancer [72,73].

Another member of the AKR1C family, AKR1C4, is mainly involved in the peripheral synthesis and metabolism of progesterone [74]. Genome-wide association studies revealed AKR1C4 is associated with human blood metabolites [75], and lipid metabolism [76]. A large-scale trans-ethnic meta-analysis found AKR1C4 is a potential candidate for age at menarche of women, which is closely associated with several diseases such as cancer [77,78], Alzheimer's disease [79], cardiovascular disease [80,81] and fatty liver [82]. Similar to AKR1C2, AKR1C4 also exhibits potential value as a biomarker of cancer. Integration AKR1C4 and Epstein-Barr virus DNA could stratify patients with nasopharyngeal carcinoma at high risk of local recurrence [83]. Through the analysis of colorectal cancer gene expression and prognosis based on the TCGA database, a prognostic model including AKR1C4 was established, providing a promising outlook for colorectal diagnosis and treatment [84].

AKR1C3 is the most extensively studied member of the AKR1C family. AKR1C3 mainly functions as a prostaglandin (PG) $F_2\alpha$ synthase and reduces $PGD_2$ and $PGH_2$ into $PGF_2\alpha$ [85]. It can also regulate the synthesis and metabolism of the androgen receptor, estrogen receptor and progesterone receptor [86]. With diverse functions in hormone metabolism and redox reactions, AKR1C3 acts as a potential therapeutic target for hormone-related carcinomas and metabolic diseases. AKR1C3 is significantly highly expressed in hepatocellular carcinoma (HCC) and associated with poor prognosis. AKR1C3 is involved in NF-κB signaling and IL6/STAT3 pathway, resulting in cell proliferation and metastasis in HCC cells [87]. AKR1C3 was also detected to regulate lipid droplet formation in HCC, further conferring sorafenib resistance, suggesting AKR1C3 might be a promising therapeutic target in HCC [88]. As a gold standard for breast cancer therapy, anthracyclines frequently encounter resistance due to AKR1C3. AKR1C3 inhibitors were

much studied recently, and co-administration significantly re-sensitized the doxorubicin (DOX) in the resistant breast cancer cell line [89]. Another study revealed aryl hydrocarbon receptor could enhance AKR1C3 promoter activity, and further cause DOX resistance, while knockdown AKR1C3 would re-sensitize DOX in triple-negative breast cancer [90]. In prostate cancer, antiandrogens are used for castration-resistant prostate cancer patients. AKR1C3 was validated as a potential upstream regulator in JNJ-pan-AR (a broad-spectrum AR antagonist) resistant cells, and overexpressing AKR1C3 could further lead to androgen receptor resistance [91]. Glutathione (GSH) is a critical antioxidant involved in reactive oxygen species (ROS) detoxification *in vivo* [92], AKR1C3 would mediate chemoresistance by regulating AKT phosphorylation and GSH level, further remove ROS in EAC [93]. In general, AKR1C3 plays a vital role in hormone metabolism and therapy resistance, which deserves further study.

### 3.2.2. The role of AKR1C3 in radiotherapy

Radiotherapy is the most-effective anti-tumor therapy available for localized solid cancer. Approximately 60% of cancer patients in the United States continue to receive radiotherapy - a century after its invention, though many other treatment approaches have emerged during this period [94]. As we mentioned before, AKR1C3 is closely associated with drug resistance; however, recent studies have shown it also plays an important role in radiotherapy [95-98].

AKR1C3 was detected with a high expression level both in non-small-cell lung cancer (NSCLC) tissues and the radioresistant NSCLC cell lines, knockdown AKR1C3 significantly sensitized IR and enhanced IR-induced apoptosis, the mechanism may be involved in IL-6-mediated signaling pathway and cell cycle arrest [95]. Another NSCLC-related study found that high AKR1C3 expression in nucleus was associated with radioresistance, and AKR1C3 expression level was positively correlated with β-catenin in nucleus [99]. Radon is a radioactive, colorless, tasteless noble gas; because of its potential radiation hazards, it is now recognized as one of the leading causes of lung cancer and leukemias [100,101]. Loiselle et al [102] performed RNA-seq on human lung epithelial cells which were exposed to radon-emitting rocks for several months, the results showed that the radon-exposed cells experienced significant changes in the gene levels of AKR1C3, suggesting that AKR1C3 may involve in radiation response and the high expression of AKR1C3 may be a risk factor for lung cancer.

In the past few years, AKR1C3 was frequently found to be upregulated in castrate resistant prostate cancer, and the administration of AKR1C3 inhibitors to treat prostate cancer has been more and more explored and reported [103-105]. Overexpressing AKR1C3 in prostate cancer cells could lead to $PGF_{2\alpha}$ accumulation and ROS level downregulation,

thus cause radioresistance, while the AKR1C3 inhibitor – indocin could re-sensitize cells to irradiation, mechanically, this AKR1C3-induced resistance might be associated with the activation of MAPK pathway [96].

AKR1C3 is also involved in the mechanism of radioresistance in ESCC. Higher expression level of AKR1C3 was detected and less IR-induced ROS accumulation was found in ESCC radioresistant cell line, AKR1C3 also prevented cells from IR-induced DNA damage, while knockdown or inhibition of AKR1C3 could rescue these effects [97]. Another study revealed that methyl jasmonate, an AKR1C3 inhibitor of $PGD_2$ 11-keto reductase activity, exhibited a strong sensitizing effect to IR in the AKR1C3 high expressed cells, while this effect was not obvious in the AKR1C3 low expressed cells [106]. Targeting AKR1C3 would be a promising strategy for ESCC treatment in radioresistant patients. While whether AKR1C3 could regulate radiosensitivity in EAC is still unclear. Previous studies by our group have validated AKR1C3 can enhance chemoresistance in EAC cells [93], further exploring the mechanism in AKR1C3 and radioresistance might have potential value in improving the prognosis of EAC patients.

Cell death induced by radiotherapy can be categorized as autophagy-dependent cell death, immunogenic cell death, apoptosis, necrosis, pyroptosis and ferroptosis [107]. Exploring the molecular mechanism of irradiation-induced cell death may be a potential approach to overcome radioresistance.

### 3.3. Ferroptosis

#### 3.3.1. Introduction

The concept of ferroptosis was first proposed by Dixon as an iron-dependent and non-apoptotic cell death [108]. Unlike other programmed cell death, ferroptosis is driven by phospholipid peroxidation with features mainly of morphological changes such as decreased mitochondria cristae, a rupture of bilayer phospholipid membrane, and a condensed mitochondrial membrane [109]. Accumulated studies suggest its potential mechanism in cancers and metabolic diseases. Numerous inducers and inhibitors of ferroptosis have been validated to regulate the level of lipid peroxidation and ROS derived from iron-induced Fenton reaction [110]. Understanding ferroptosis from multiple perspectives such as molecular mechanisms, signaling pathways, cell morphological changes, and mitochondrial functions may provide new diagnostic and therapeutic approaches to improve the prognosis in cancers.

The balance of intracellular antioxidant metabolism is regulated by the dynamic synergy of many factors such as glutathione peroxidase 4 (GPX4), coenzyme Q10 (CoQ), ferroptosis inhibitor protein 1 (FSP1) and dihydroorotate dehydrogenase (DHODH) [111-

[113]. GPX4 and CoQ are two independent signaling pathways of antioxidant metabolism (Figure 1). GPX4 inhibits ferroptosis by detoxifying lipid peroxidation through the following chemical reactions:

$$GSH + L\text{-}OOH \xrightarrow{GPX4} GSSG + L\text{-}OH$$

As a pivotal reductant in organisms, Glutathione (GSH) can reduce phospholipid hydroperoxides (L-OOH) into phospholipid alcohols (L-OH) under the catalyzing effect of GPX4, thereby avoiding the occurrence of ferroptosis [114]. The synthesis of GSH depends on cystine, and cystine needs the help of xCT system (SLC7A11 and SLC3A2) to be taken up into the cell [115]. Recent studies have confirmed that SLC7A11 is the key hub for regulating ferroptosis [116-118]. Erastin and RAS-selective lethal 3 (RSL3), as wildly studied ferroptosis inducers, inhibit SLC7A11 and GPX4, respectively, leading to accumulation of lipid peroxidation and eventually causing ferroptosis [119].

CoQ is another vital ferroptosis defense system which is parallel to the SLC7A11/GSH/GPX4 pathway. Its reduced form of $CoQH_2$ plays an antioxidant role in plasma membrane and mitochondrial membrane, reduce phospholipid hydroperoxides, and protect cells from ferroptosis [111,113,120]. Ferroptosis inhibitor protein 1 (FSP1), previously known as apoptosis-inducing factor mitochondrial 2 (AIFM2), could be recruited through N-terminal myristoylation to the plasma membrane where it reduces the oxidized form of CoQ to the reduced form of CoQ ($CoQH_2$) as a reductase. $CoQH_2$ further blocks the accumulation of lipid peroxidation independently from GPX4 [111]. Recently a new study from MD Anderson Cancer Center revealed another metabolic pathway of CoQ in mitochondria [113]. Dihydroorotate dehydrogenase (DHODH) is an enzyme located on the outer side of the inner mitochondrial membrane [121]. Similar to FSP1, DHODH also functions as an oxidoreductase to reduce CoQ to $CoQH_2$, thus prevents mitochondrial membrane from oxidative damage.

Iron metabolism and lipid metabolism are also involved in the mechanism of ferroptosis [122,123]. In addition, crosstalk between ferroptosis and canonical signaling pathways has been reported, providing more therapy targets in different types of cancer [124-129].

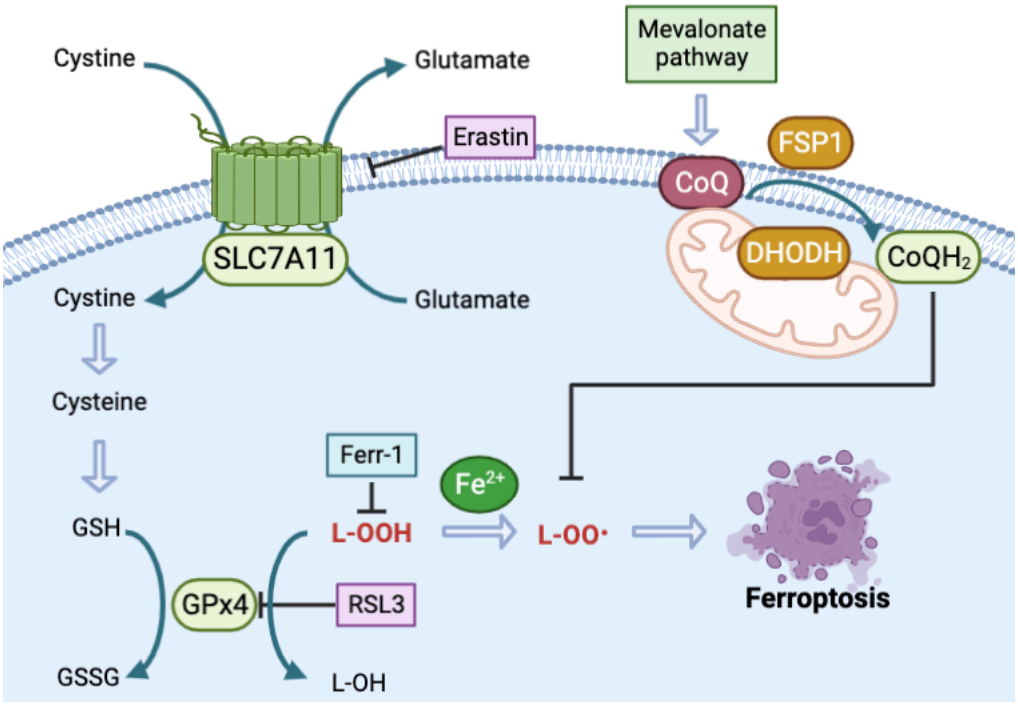


**Fig 3.3.1 Two major pathways of ferroptosis**

SLC7A11/GSH/GPX4 and CoQ are the two major ferroptosis defense systems. As a raw material for GSH synthesis, cystine is taken up into cells by xCT and further synthesized into GSH. GSH and L-OOH undergo redox reactions under the catalysis of GPX4 to generate GSSG and L-OH, respectively. CoQ can be reduced to $CoQH_2$ by FSP1 and DHODH in plasma membrane and mitochondrial membrane, respectively. $CoQH_2$ continues to function as a lipid ROS scavenger in membrane.

### 3.3.2. Ferroptosis in Cancer

Mounting studies reveal that ferroptosis is a programmed cell death which is vital for eradicating the cancer cells [130]. Previous evidences show that p53 exhibits its capacity to regulate cell cycle arrest, apoptosis and energy metabolism [131]. However, p53 could also mediate ferroptosis by directly inhibiting SLC7A11 through binding to the promotor. Obvious difference between the effects of p53-null cells versus p53+/+ or $p53^{3KR/3KR}$ mouse embryonic fibroblasts detected at different time points with the co-culture to different concentrations of erastin [132]. Another study showed wild-type p53 could delay ferroptosis in response to cystine deprivation [133]. In general, oncogene activation and tumor suppressor inactivation can regulate ferroptosis either positively or negatively, depending on the pathway affected and the cellular context [134].

In recent years, due to the potential therapeutic prospect, ferroptosis inducers (FINs) has been more and more developed and researched. Additionally, nanoparticle inducers have attracted a lot of attention for cancer therapy, especially for the drug resistant cases [135]. Given the unsatisfied therapeutic efficiency, outcome, and clinical translation of the

nanomaterials, a deep mining of nano–bio interaction is required [136]. Mounting evidences suggest ferroptosis is involved in the response of chemotherapy, radiotherapy, and immunotherapy [92,137-139], combination FINs with nanomaterials into cancer therapy would be a promising strategy manage cancers.

### 3.3.3. The role of ferroptosis in radiotherapy

Radiotherapy is one of the major anti-tumor approaches, while the growing rate of radioresistance results in clinical treatment failure [140]. RT could upregulate ROS in cytoplasm, mitochondria and plasma membrane by the radiolysis of cellular water and the activation of oxidoreductases, such as the peroxides, singlet oxygen and hydroxyl radical, which may damage DNA, proteins, and membranes [141]. As we mentioned before, ROS would lead to lipid peroxidation in plasma membrane further cause ferroptosis. Radiotherapy now is also defined as an inducer of ferroptosis due to its radiolysis of water [142]. Further exploration FINs in the application for radioresistant cancers would be promising.

Kelch-like ECH associated protein 1(KEAP1) is detected as a frequently mutated or inactivated gene in lung cancer, and mutated KEAP1 usually result in radioresistance. Inhibition of FSP1 would re-sensitize KEAP1 deficient cells / patient-derived xenografts to radiotherapy, this study suggests FSP1 is a vital downstream target of KEAP1-NRF2 signaling pathway [139]. SLC7A11 is also proved to be a potent ferroptotic target against radioresistance in lung cancer. The RNA-binding protein RBMS1 can regulate the translation of SLC7A11 then inhibit ferroptosis, the selective inhibitor of RBMS1/SLC7A11 axis significantly re-sensitizes the radioresistant lung cancer cells to RT via ferroptotic activation [143]. Inhalation of drug-loaded smart nanoclusters with targeted modifications through the intratracheal can improve the therapeutic effect for lung cancer patients [144]. Small pieces of self-assembled pH-sensitive superparamagnetic iron oxide nanoclusters (SPIONCs) reach deeply into the lung cancer and release more iron ions, while big pieces cannot pass through the upper airway. With the stimulation of irradiation, accumulated iron ions can intensify Fenton reaction to generate more ROS, further cause ferroptosis [145]. For tumors that are difficult to reach with general drugs or radiotherapy, nanomaterials provide a new therapeutic approach.

Growing studies found ferroptosis is associated with radioresistance in esophageal cancer. NRF2 and SLC7A11 were detected overexpressed in ESCC and positively correlated with each other. By ChIP-sequencing analysis, NRF2 was validated to bind to the promoter of SLC7A11 directly, further mediating the expression of SLC7A11. SLC7A11 induced by hyperactive NRF2 could lead to radioresistance via suppressing ferroptosis, while silencing of SLC7A11 re-sensitized ESCC cells to irradiation [146]. As an

important enzyme responsible for reducing saturated fatty acid to monounsaturated fatty acid, Stearoyl-CoA desaturase 1 (SCD1) is confirmed as a promising target to sensitize ESCC to irradiation [147]. Another newly validated gene - stanniocalcin 2 (STC2), contributed to radioresistance in ESCC by activating protein methyltransferase 5 through regulation of DNA damage repair and ferroptosis [148]. So far, we have found a considerable number of studies on ferroptosis and radioresistance in ESCC, but the ferroptotic mechanism of radioresistance in EAC is still unclear. With the emergence of clinical treatment resistance, deep learning of ferroptosis in EAC may have the potential to improve prognosis.

## 4. AIM OF THE STUDY

In this study, we will establish a unique model to study radioresistance of EAC in vitro. Then perform RNA-sequencing analysis to compare the radioresistant model, to find the different expressed genes. We will validate whether AKR1C3 could enhance radioresistance and inhibit IR-induced ferroptosis in EAC cells. Lastly, we will check whether cells could be re-sensitive to irradiation after AKR1C3 targeting treatment.

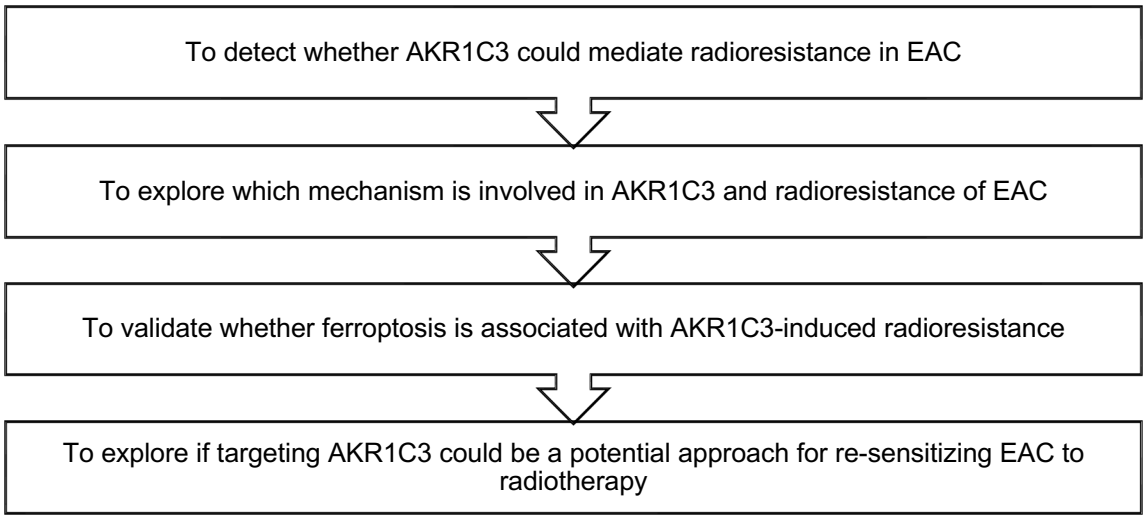

# 5. MATERIALS AND METHODS

## 5.1. Materials

### 5.1.1. Cell lines

The human EAC cell lines SKGT-4, FLO-1 and OACP4C were kindly provided by Prof. Axel M. Hillmer from the Laboratory of Genomic Pathology at the Institute of Pathology of University of Cologne (Cologne, Germany), while OE33 was obtained from the Sigma Cell Line Bank (Sigma, 96070808). All the EAC cell lines were maintained in RPMI1640 medium (Life technology, Germany) with 10% fetal bovine serum (FBS) (Invitrogen, Carlsbad, CA, USA), penicillin and streptomycin (100 U/mL penicillin + 0.1 mg/mL streptomycin) (PAN Biotech, Aidenbach, Germany) in a humidified atmosphere of 5% CO2 at 37 °C. Furthermore, all cell lines were tested and confirmed free from mycoplasma contamination.

### 5.1.2. Materials for cell culture

| Materials | Company |
|---|---|
| RPMI1640 | Life technology, Germany |
| Fetal bovine serum (FBS) | Cat#FBS12-A, Capricorn Scientific GmbH, Germany |
| Penicillin-Streptomycin (10 units/mL of penicillin and 10 µg/mL of streptomycin) | Cat#15140122, Gibco Invitrogen, Germany |
| Trypsin-EDTA 0.25%, phenol red | Cat#25200056, Gibco Invitrogen, Germany |
| Doxycycline hyclate | Cat#2431450, Peprotech, Germany |
| Trypan blue stain (0.4%) | Cat#T10282, Invitrogen, Germany |
| Dimethylsulfoxide (DMSO) | Cat#A36720100, AppliChem, Germany |
| Dulbecco's phosphate-buffered saline (DPBS) | Cat#14190094, Gibco Invitrogen, Germany |

### 5.1.3. Medium for cell culture and cryopreservation

#### 5.1.3.1. Medium for cell culture

| Medium | Supplements |
|---|---|
| OE33, SKGT-4 | |
| RPMI1640 | 10% FBS<br>0.1 units/mL Penicillin<br>1 µg/mL Streptomycin |

#### 5.1.3.2. Medium for cryopreservation

| | |
|---|---|
| FBS (90%) | DMSO (10%) |

### 5.1.4. Materials for PCR

#### 5.1.4.1. RNA extraction

| Name | Company |
|---|---|
| NucleoSpin® Tissue | Cat# 740952, MACHEREY-NAGEL, Germany |
| TRI reagent | Cat# T9424, Sigma, Germany |
| NucleoSpin® Gel and PCR Clean-up | Cat# 740609, MACHEREY-NAGEL, Germany |
| AllPrep DNA/RNA/Protein Mini Kit | Cat# 80004, QIAGEN, Germany |

#### 5.1.4.2. Quantitative real-time PCR

| Name | Company |
|---|---|
| High-Capacity cDNA Reverse Transcription Kit | Cat#4368814, Applied Biosystems, USA |
| Fast SYBR™ Green Master Mix | Cat#4385612, Applied Biosystems, USA |

| | |
|---|---|
| MicroAmp™ Clear Adhesive Film | Cat#4306311, Applied Biosystems, USA |
| MicroAmp™ Optical 96-Well Reaction Plate | Cat#N8010560, Applied Biosystems, USA |

### 5.1.5. Materials for protein analysis

#### 5.1.5.1. Reagents

| Name | Company |
|---|---|
| RIPA Buffer (10X) | Cat#9806, Cell Signaling Technology, USA |
| Pierce™ BCA Protein Assay Kit | Cat#23225, Thermo Scientific™, Germany |
| PMSF Protease Inhibitor | Cat#36978, Thermo Scientific™, Germany |
| Pierce™ LDS Sample Buffer, Non-Reducing (4X) | Cat#84788, Thermo Scientific™, Germany |
| PageRuler™ Prestained Protein Ladder 10 to 180 kDa | Cat#26617, Thermo Scientific, Germany |
| SuperSignal™ West Pico PLUS Chemiluminescent Substrate | Cat#34577, Thermo Scientific, Germany |
| Roti®-Block (10X) | Cat#A151,2, Carl Roth, Germany |

#### 5.1.5.2. Buffers

| **Running buffer, pH 8.3** |
|---|
| Tris (25 mM) |
| Glycine (190 mM) |
| SDS (0.1%) |
| dd$H_2O$ |

| **Transfer buffer, pH 8.3** |
| --- |
| Tris (25 mM) |
| Glycine (190 mM) |
| Methanol (10%) |
| dd$H_2O$ |

| **Washing buffer (TBST), pH 7.4** |
| --- |
| Tris (20 mM) |
| Sodium Chloride (150 mM) |
| ddH2O |
| Adjust pH to 7.4 with HCl |
| Tween-20 (1:1000) |

| **Blocking buffer** |
| --- |
| Roti-Block (10X) |
| dd$H_2O$ |

| **Primary antibody dilution solution** |
| --- |
| Roti-Block (10X) |
| BSA (0.1%) |
| Sodium azide (0.05%) |

| |
|---|
| $ddH_2O$ |

| **Striping buffer** |
|---|
| Glycine (20 mM) |
| SDS (1%) |
| Adjust pH to 2.0 with HCl |
| $ddH_2O$ |

#### 5.1.5.3. Antibodies

| Antibody | Company | Catalog | Specificity | Host |
|---|---|---|---|---|
| α-tubulin | Cell signaling technology | 3873 | Human | Mouse |
| AKR1C3 | R&D Systems<br>Abcam | MAB7678<br>ab209899 | Human | Mouse<br>Rabbit |
| SLC7A11 | Cell signaling technology | mAb#12691 | Human | Rabbit |
| GPX4 | Abcam | ab125066 | Human | Rabbit |
| H2AX | ThermoFisher scientific | MA1-2022 | Human | Mouse |
| 2nd antibody | Invitrogen | 31430 | Mouse | Goat |
| 2nd antibody | Invitrogen | 31460 | Rabbit | Goat |

### 5.1.6. Materials for comet assay and electrophoresis

#### 5.1.6.1. Reagents

| Name | Company |
|---|---|
| Agarose Low Melt | Nr. 6351.1, Carl Roth, Germany |

| | |
|---|---|
| Agarose Normal Melt | Cat#9012-36-6, Merck KGaA, Germany |
| DNA Gel Loading Dye (6X) | Cat#R0611, Thermo Scientific™, Germany |
| Nancy-520 | Cat#01494, Sigma, Germany |
| DNA Ladder (100 bp) | Cat#P087, New England Biolabs, England |

#### 5.1.6.2. Buffers

| **TBE buffer pH 8.3** |
|---|
| Tris (100 mM) |
| Boric acid (100 mM) |
| EDTA (2 mM) |
| $ddH_2O$ |

| **Neutralization buffer pH 7.5** |
|---|
| Tris (400 mM) |
| HCl (for pH adjustment) |
| $ddH_2O$ |

### 5.1.7. Materials for plasmids construction and lentiviral transduction of mammalian cells

| Name | Company |
|---|---|
| CutSmart® Buffer | Cat#B7204S, New England Biolabs, England |
| NEBuffer™ 2 | Cat#B7002S, New England Biolabs, England |
| T4 DNA Ligase | Cat#M0202S, New England Biolabs, England |

| | |
|---|---|
| AgeI-HF | Cat#R3552S, New England Biolabs, England |
| XhoI-HF | Cat#R0146S, New England Biolabs, England |
| EcoRI-HF | Cat#R3101S, New England Biolabs, England |
| pMDLg/pRRE | Cat#12251, Addgene, USA |
| pMD2.G | Cat#12259, Addgene, USA |
| pRSV-Rev | Cat#12253, Addgene, USA |
| Tet-pLKO-puro | Cat#21915, Addgene, USA |
| Polyethylenimine, branched (PEI) | Cat#408727, Sigma, Germany |
| Hexadimethrine bromide/polybrene | Cat#H9268, Sigma, Germany |
| Puromycin | Cat#5855822, PeproTech, USA |
| Ampicillin Trihydrat | Cat#SIALA1593, VWR, Germany |
| Mix & Go! Competent Cells-TG1 | Cat#T3017, Zymo Research, USA |
| NucleoSpin® Plasmid | Cat#740588, MACHEREY-NAGEL, Germany |
| NucleoBond® Xtra Midi | Cat#740412, MACHEREY-NAGEL, Germany |
| LB Broth (without agar) | Cat#L2542, Sigma, Germany |
| LB Broth (with agar) | Cat#L3147, Sigma, Germany |

### 5.1.8. Materials for flow cytometry

#### 5.1.8.1. Reagents and staining dyes

| Name | Company |
|---|---|

| | |
|---|---|
| Tetramethylrhodamine ethyl ester (TMRE) | PK-CA707-70016, PromoCell GmbH, Germany |
| APC Annexin V | Cat#640920, Biolegend, USA |
| DAPI (4 ', 6-diamidino-2-phenylindole, dihydrochloride) | Cat#62247, Thermo Scientific, Germany |
| MitoSox - Mitochondrial Superoxide Indicators | Cat#M36008, Thermo Scientific, Germany |
| BODIPY™ 581/591 C11 | Cat#D3861, Thermo Scientific, Germany |

#### 5.1.8.2. Buffers for flow cytometry

| **Annexin V Binding buffer** |
|---|
| 10 mM HEPES, pH 7.4 |
| 150 mM NaCl |

| | |
|---|---|
| Gey's Balanced Salt Solution | Cat#G9779, Sigma-Aldrich, Germany |

### 5.1.9. Materials for Co-immunoprecipitation (Co-IP)

#### 5.1.9.1. Reagents

| Name | Company |
|---|---|
| Dynabeads™ Protein G for Immunoprecipitation | Cat#10004D, Invitrogen, Germany |
| Dynabeads™ Protein A for Immunoprecipitation | Cat#10002D, Invitrogen, Germany |
| Normal mouse IgG | Cat#sc-2025, Santa Cruz Biotechnology, Germany |
| Normal Rabbit IgG | Cat#sc-2025, Merck KGaA, Germany |

#### 5.1.9.2. Buffers

| **Lysis buffer / dilution buffer** | |
|---|---|
| Cell Lysis Buffer (1X) | Cat#9803, Cell signaling technology, Germany |
| PMSF Protease Inhibitor (1:200) | Cat#36978, Thermo Scientific™, Germany |

| **Washing buffer** |
|---|
| DPBS |
| Tween 20 (0.05%) |

#### 5.1.9.3. Antibodies

| **Antibody** | **Company** | **Catalog** | **Specificity** | **Host** |
|---|---|---|---|---|
| AKR1C3 | Abcam | ab209899 | Human | Rabbit |
| SLC7A11 | Cell signaling technology | mAb#12691 | Human | Rabbit |
| GPX4 | Abcam | ab125066 | Human | Rabbit |

### 5.1.10. Materials for Seahorse experiments

| Name | Company |
|---|---|
| Seahorse XF Cell Mito Stress Test Kit | Nr: 103015-100, Agilent Technology, USA |
| Seahorse XF Glycolysis Stress Test Kit | Nr: 103020-100, Agilent Technology, USA |

### 5.1.11. Chemicals and chemotherapy agents

#### 5.1.11.1. Chemicals

| Name | Company |
|---|---|

| | |
|---|---|
| MTT | Cat#cay- 21795, Biomol, Germany |
| Albumin Fraction V (BSA) | Cat#8076.2, Carl Roth, Germany |
| Tris | Cat#9127.2, Carl Roth, Germany |
| SDS | Cat#A72495000, AppliChem, Germany |
| TCEP | Cat#C4706, Sigma, Germany |
| Sodium azide | Cat#8690, Th. Geyer, Germany |
| Chloroform | Cat#C7559, Sigma, Germany |
| Sodium Chloride | Cat#3957.2, Carl Roth, Germany |
| Tween 20 | Cat#9127.2, Carl Roth, Germany |
| Triton X-100 | Cat#8013, Th. Geyer, Germany |
| Nonidet® P40 | Cat#A1694, AppliChem, Germany |
| EDTA | Cat#E-5134, Merck, Germany |
| Hydrochloric acid (2N) | Cat#182108, Th. Geyer, Germany |
| Sodium hydroxide (1N) | Cat#1340, Th. Geyer, Germany |
| 2-Propanol (99%) | Cat#9866.5, Carl Roth, Germany |
| Ethanol (99%) | Cat#2212, Th. Geyer, Germany |
| Methanol | Cat#4627.5, Carl Roth, Germany |

**5.1.11.2. Therapy agents**

| Name | Company |
|---|---|
| Erastin | Cat#Cay17754-1, Biomol, Germany |

| | |
|---|---|
| Ferrostatin-1 | Cat#SML0583, Merck KGaA, Germany |
| Medroxyprogesterone acetate | CAS: 71-58-9, Thermo scientific, USA |
| Z-VAD-FMK | CAS: 187389-52-2, Merck KGaA, Germany |

### 5.1.12. Laboratory equipments

| Name | Company |
|---|---|
| Class II Safety Cabinets | Herasafe KS, Thermo Scientific™, Germany |
| BIOBEAM GM 8000 | Gamma-Service Medical GmbH, Germany |
| CO2-incubators Heracell 150i, | Thermo Scientific™, Germany<br>MCO-230AICUV-PE, Panasonic, Japan |
| Centrifuge | Megafuge 1.0R, Heraeus, Germany |
| Microcentrifuge | Thermo Scientific™, Germany |
| Automatic pipettes | Eppendorf, Germany |
| Vortex | Lab dancer, VWR, Germany |
| Phase Contrast Microscope | DFC450C, Leica, Germany |
| IX83 Inverted Microscope | Olympus, Japan |
| Automated Cell Counter | Countess II, Invitrogen, USA |
| Attune NxT Flow Cytometer | ThermoFisher scientific, USA |
| Seahorse XFe96 Analyzer | Agilent Technology, USA |
| Fridge 4°C | Liebherr, Germany |
| Freezer -20°C | Bosch, Germany |

| | |
|---|---|
| Freezer (-80°C and -150°C) | Sanyo, Japan |
| Plate Reader | FLUOstar Omega, BMG Labtech, Germany |
| CellCamper® Mini, freezing box | NeoLab, Germany |
| Water bath | Störk-Tronic, Germany |
| Mini-PROTEAN® System | Bio-Rad, USA |
| Trans-Blot® Turbo™ Transfer System | Bio-Rad, USA |
| INTAS ECL CHEMOSTAR | Intas Science Imaging, Germany |
| Thermocycler | Tpersonal, Biometra, Germany |
| Thermomixer | ThermoMixer C, Eppendorf, Germany |
| Spectrophotometer | NanoDrop One, Thermo Scientific™, Germany |
| Real time PCR | QuantStudio 7 flex, Applied Biosystems, USA |
| Sonicator | Bioruptor® Pico, Diagenode, Belgium |

### 5.1.13. Consumable materials

| Name | Company |
|---|---|
| Tube (5, 15 and 50mL) | Sarstedt, Germany |
| SafeSeal tube | Sarstedt, Germany |
| Centrifuge tube (15 and 50ml) | Sarstedt, Germany |
| Cryotubes (1.8 mL) | Sarstedt, Germany |
| Serological pipettes (5, 10 and 25mL) | Sarstedt, Germany |

| | |
|---|---|
| Pipette tips (10, 200 and 1000µL) | Sarstedt, Germany |
| Tissue culture dish, (ØxH): 100 x 20 mm, 30 x 10 mm | Sarstedt, Germany |
| Cell culture flask, T-25, T-75, surface: Cell+, Filter cap | Sarstedt, Germany |
| Cell culture plates (6, 12, 24 and 96-well) | Sarstedt, Germany |
| Cell culture chamber (8 well) | Sarstedt, Germany |
| Western Blotting Filter Paper, Extra Thick, 8.5 cm x 9 cm | Cat# 88610, Thermo Scientific, Germany |
| PVDF membrane (0.2µM) | Cat# 741260, MACHEREY-NAGEL, Germany |
| Cell counting slide | Cat# 734-2676, VWR, Germany |
| Syringe filters (0.2 and 0.45µm) | Cat# 512-3180/3182, VWR, Germany |
| Cell strainer (40, 70 and 100 µm pore size) | Cat# 734-2760, VWR, Germany |

### 5.1.14. Software

| Name | Company |
|---|---|
| Microsoft Office | Microsoft Corporation, USA |
| macOS Ventura (13.0.1) | Apple, USA |
| ImageJ / Fiji | National Institutes of Health, USA |
| GraphPad Prism 9 | GraphPad Software, Inc., USA |
| Endnote X20 | Thomson Reuter, U.S.A. |
| RStudio 4.2.1 | Posit Software, USA |

| | |
|---|---|
| FlowJo | BD, USA |
| Wave Desktop | Agilent Technology, USA |

## 5.2. Methods

### 5.2.1. Cell culture

EAC cells were cultured in the 10 cm dish or T-25 / T-75 flask in the incubator, with a humidified air of 5% $CO_2$ at 37 °C. Medium is changed every 2-3 days. Cells were passaged from 1:3 to 1:10 according to a different growth speed of the cells when they reached the confluence of 75%-95%.

For passage, the medium was removed from the dish, and DPBS was added for washing. Then 0.25% Trypsin-EDTA was used for digestion. After 3-5 mins, the medium was added, then pipette several times, choose the appropriate passage ratio according to the requirement of the experiment.

For storage, firstly, cells were collected by trypsinization and centrifugation; cell counting were done during this step. Then, cells were resuspended in cryopreservation medium, and every two million cells mixed with 1 mL cryopreservation medium were aliquoted into a tube. The tubes were removed into a CoolCell LX Freezing Container and kept in a -80 ℃ freezer for short-term storage. The aliquots were transferred from the -80 ℃ freezer the next day into the -150 ℃ freezer for long-term storage.

For re-cultivation, cells were taken out of the -80 ℃ / -150 ℃ freezer and put into the 37 ℃ water bath immediately. After complete thawing (usually 1-2 mins), cells were removed into a 15mL tube with 10mL prewarmed medium inside then pelleted by centrifugation, afterwards the supernatant was discarded. Lastly, cells were re-suspended with the pre-warmed medium and transferred into the 10 cm dish.

### 5.2.2. Cell counting

Countess II Automated Cell Counter (Invitrogen) was used for the cell counting. The procedure was as follows: after collecting and resuspending the cells, mix 20 µL of the cell suspension and 20 µL of the trypan blue solution with a pipette. Then transfer 10 µL of the mixture to a Countess chamber slide and insert into Countess II Automated Cell Counter. Cell concentration and viability are determined and shown directly on the screen.

### 5.2.3. Establishment of the radioresistant cell line

OE33 was chosen for the radioresistant cell line establishment. Two flasks of cells from the same dish of OE33 were labeled as OE33P (the parental cell line) and OE33R (the radioresistant cell line). OE33R received 2 Gy gamma ray once it reached 50 - 70% confluence (BIOBEAM GM 8000, Gamma-Service Medical GmbH, Germany). OE33P was mock-irradiated (in order to ensure the same environment as OE33R). Cells were passaged when they reached 90% confluence. After 23 cycles (46 Gy in total), the cells rested for 3 weeks before proceeding to the next experiments. To validate the models, colony formation was performed, the averaged data were fitted into single-hit multi-target formula: $S= 1 - (1 - e^{-D/ D0})^N$. S is the fraction of cells surviving, $D_0$ is the "mean lethal dose", the dose on the straight-line portion of the survival curve to decrease the survival to 37%. Dq is the quasi-threshold dose, is the width of the "shoulder," and correlates with repair capacity. N is the extrapolation number.

### 5.2.4. Colony formation assay

EAC cells (300 – 2 × $10^3$ cells / well) were seeded in 6-well plates with 2 mL full RPMI 1640 medium each well at 37˚C with 5% $CO_2$. After 24 hours, test groups were treated with irradiation or related agents, while control groups were under mock treatment. After 7 - 14 days, when the complete colonies were formed, remove the medium, wash once with DPBS, then fix with formalin at room temperature for 30 minutes, then stain with crystal violet (Sigma-Aldrich, Germany) for 20 minutes, and finally wash gently with water twice, then let them dry. Colonies with more than 50 cells were recorded under the microscope (Leica, DMIL, Germany).

### 5.2.5. Immunofluorescence

EAC cells were seeded in 8-well chamber slides (ibidi) with 2 - 4 x $10^4$ / well and incubated at 37˚°C with 5% $CO_2$ for 24h. Then the test groups were irradiated with 3 - 8 Gy. After another 24h, the cells were gently washed with PBS twice. Then fix the cells with 4% formalin for 15 min, wash with PBS 5 min x 3 times, permeabilize with 0.2% Triton X-100 for 15 min, wash with PBB (PBS + 0.5% BSA) 5 min x 3 times, then block with normal serum block for 40 min at room temperature, wash with PBB once for 5 min. Then cells were incubated with primary antibody of anti-H2AX (1:800) overnight at 4°C. The next morning, cells were washed with PBB 5 min x 3 times, then incubated with secondary antibody (Alexa 488-conjugated anti-mouse, 1:1000) for 1h at RT. DAPI (1:4000) was also stained for nuclear staining for 5 min. Afterwards, wash cells 5 min x 3 times, cover slides with mountain medium and keep them in darkness. Images were taken with IX83 Inverted Microscope. Further image processing was done by ImageJ.

### 5.2.6. Quantitative Real-time PCR (qRT-PCR)

TRI reagent (Sigma-Aldrich, Germany) was used for extracting total RNA from the cultured EAC cells. Then, the High-Capacity cDNA Reverse Transcription Kit (Applied Biosystems, Thermo Fisher Scientific, USA) was used for cDNA synthesis according to the manufacturer's protocol. Primers are listed (Table 4.1). Relative expression of target mRNAs was measured by using Fast SYBR Green Master Mix (Invitrogen) with QuantStudio 7 Flex (Applied Biosystems, Thermo Fisher Scientific, USA) and analyzed by the delta-delta-CT method.

**Table 4.1** Primers for qRT-PCR

| Gene | Sequence (5' to 3') |
|---|---|
| GAPDH-for | GAAGGTGAAGGTCGGAGTC |
| GAPDH-rev | GAAGATGGTGATGGGATTTC |
| hAKR1C3-for | GTCATCCGTATTTCAACCGGAG |
| hAKR1C3-rev | CCACCCATCGTTTGTCTCGTT |

### 5.2.7. Western blot

Cells were harvested and lysed with RIPA buffer supplemented with protease and phosphatase inhibitors when the dishes reached 95% confluence. Then, cell lysates were sonicated for 5 min, then centrifuged at 13000× g for 10 minutes at 4°C. The supernatant was collected, and the protein concentration was then measured by BCA protein assay (Thermo Fisher Scientific). Protein was cooked with bolt loading buffer in 1x NuPAGE LDS sample buffer (Invitrogen) at 70 ℃ for 10 min. Twenty microgram protein samples were electrophoresed for 80-90 min in the SDS-PAGE gel (Tris-Glycine, self-made) and transferred to PVDF membrane (MA-CHEREY-NAGEL, Germany) by semi-dry electroblotting (Bio-Rad, Singapore). The membranes were blocked for 1 h in 1× Roti-Block buffer (Carl Roth, Germany) at RT on the shaker, then incubated with specific primary antibodies at 4 °C overnight on the rotator. Membrane was incubated with HRP-conjugated secondary antibody (Invitrogen, 31430 and 31460) for 1h at RT and visualized with SuperSignal West Pico PLUS Chemiluminescent Substrate (Thermo Fisher Scientific, USA) and detected by ChemoStar ECL Imager (Intas Science Imaging, Germany).

### 5.2.8. Flow cytometry analysis

For the apoptosis analysis, cells were treated with irradiation for 6-10 Gy. After 48h, cells (including the floating cells) were harvested by trypsinization, then incubated in

annexin V binding buffer, with annexin V (BioLegend, USA) and DAPI staining at RT for 20 min. Then, samples were washed with binding buffer twice.

For the C11-Bodipy assay, cells were treated with irradiation or erastin. After 48h, cells were harvested and stained with 1μM C11-Bodipy and DAPI for 15min at 37 ℃. Cells were then washed twice with PBS.

Experiments are performed on Attune NxT Flow Cytometer. Data analysis is done with FlowJo software (Tree Star, Ashland, USA).

### 5.2.9. Publicly available data analysis

The public database TCGA (http://cancergenome.nih.gov/) and FerrDb2 (http://www.zhounan.org/ferrdb/current/) were used to analyze prognosis and ferroptosis-related genes in EAC. Survival analysis was performed using the Kaplan–Meier method and the difference was tested with the log-rank test. A $p$-value < 0.05 was considered statistically significant.

### 5.2.10. RNA sequencing and data analysis

OE33P and OE33R triplicates were cultured and kept in a good condition. AllPrep DNA/RNA/Protein Mini Kit was used for the RNA extraction. Samples were sent to Macrogen Europe (Amsterdam, Netherlands) for total RNA sequencing. RNA-seq was performed by Illumina- NovaSeq 6000. The quality control of the raw data was finished by FastQC. Trimmomatic was used for trimming reads and removing adapter sequences. BWA-MEM, Samtools and FeatureCounts were applied for the next analysis. The following R packages were used for further data analysis and the graphing of volcano plot, heatmap and dotplot: ggplot2, ggrepel, ggpubr, DOSE, clusterProfiler, org.Hs.eg.db, enrichplot, pathview, ggnewscale, pheatmap, DESeq2 and dplyr.

### 5.2.11. Statistical analysis

Statistical analysis was finished by GraphPad Prism 9. The Kaplan–Meier method was used to calculate the overall survival. Data was presented as mean ± SD, * $p$ < 0.05, ** $p$ < 0.01, *** $p$ < 0.001, ns: non-significant, $p$ > 0.05. Statistical significance was determined by two-sided unpaired t-test.

# 6. RESULTS

## 6.1. Establishment and validation of the radioresistant EAC cell line model

### 6.1.1. Establishment of the radioresistant EAC cell line model

In order to deeply explore the mechanism of EAC and radioresistance, we decided to establish a radioresistant model of EAC cell line. The setup of the radioresistant model was referred to Dr. Maher, who was the first one successfully established the radioresistant EAC cell line model as we know [45]. OE33 cells were subcultured into two plates, labeled as OE33P (the parental cell line) and OE33R (the radioresistant cell line). OE33R was exposed to 2 Gy of gamma-ray irradiation each time when it reached 50 - 70% confluence. We passaged the cells when they grew to 90% confluence (Figure 6.1.1. A). Generally, a rest period of 7-10 days was required between two irradiation treatments. When 25 cycles were completed, which means a total dose of 50 Gy, the cells rested for one week. Then we performed a single-cell colony formation experiment on OE33R, and after one week, we selected a healthy colony as the radioresistant model of OE33R. During the establishment process, in order to ensure the accuracy of the model, OE33P was always in the same environment and conditions as OE33R.

### 6.1.2. Validation of the radioresistant EAC cell line model *in vitro*

To validate the radioresistant model in vitro, colony formation assay was performed in OE33P and OE33R. 300 - 1200 cells were seeded in the 6-well plates, then received 0 - 6 Gy irradiation after 24h. OE33R had obviously higher survival fraction than OE33P at 2, 4 and 6 Gy (Figure 6.1.1. B, D). The single-hit multi-target model was applied to this model, showing that the $D_0$ and $D_q$ values of OE33R were significantly higher than the parental cell line OE33P (Figure 6.1.1. C). We further performed RNA-seq for OE33P / OE33R, the sequencing data showed AKR family genes (AKR1C1, AKR1C2, AKR1C3 and AKR1C4) were significantly upregulated in OE33R compared to OE33P (Figure 1. E, F). Interestingly, SLC7A11, a ferroptosis-related gene, was also highly expressed in OE33R. Then, we validated AKR1C3 expression in OE33P and OE33R by qRT-PCR and Western blot, both of them indicated a high expression level of AKR1C3 in OE33R (Figure 6.1.1. G, H).

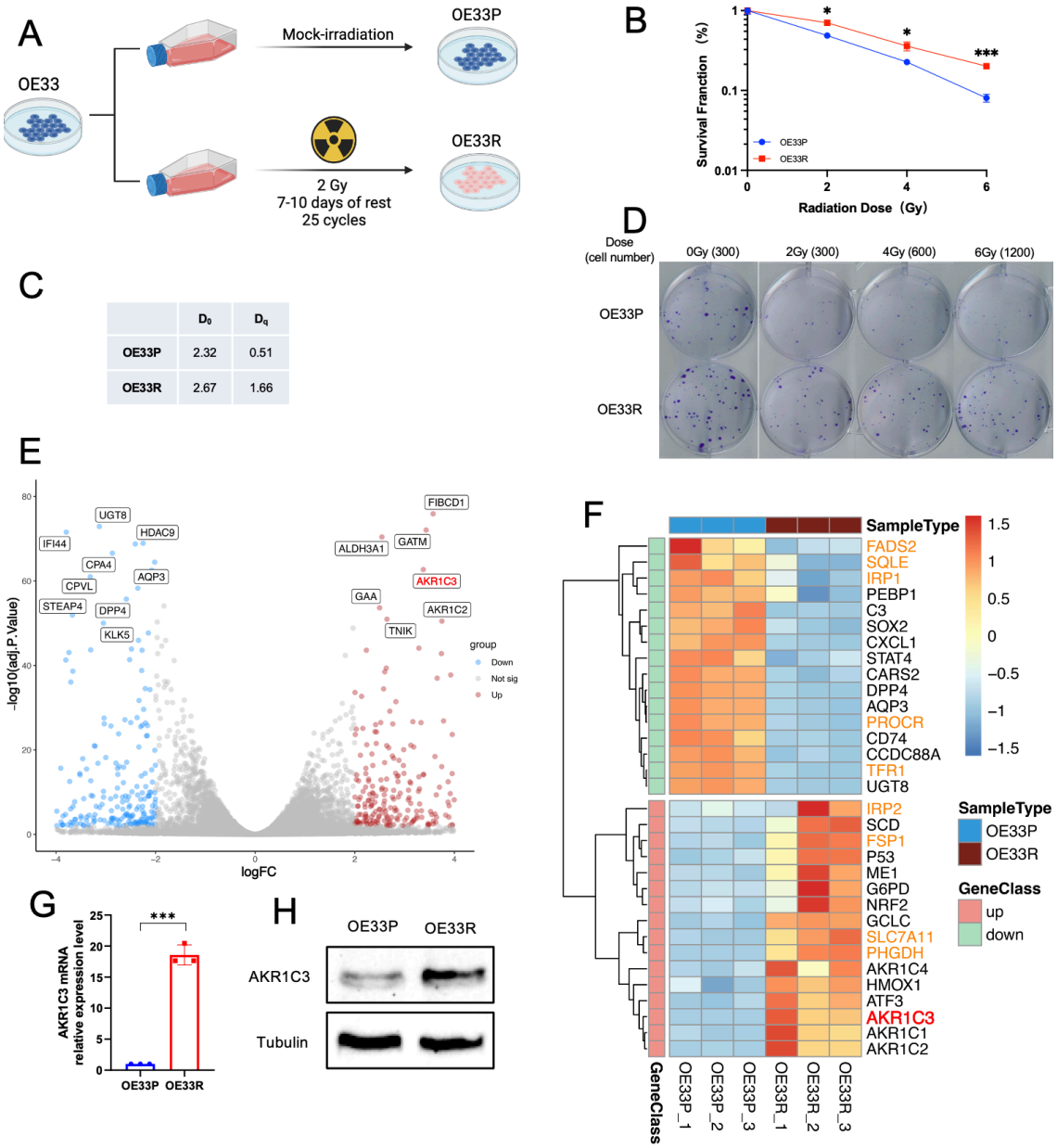


| | $D_0$ | $D_q$ |
|---|---|---|
| **OE33P** | 2.32 | 0.51 |
| **OE33R** | 2.67 | 1.66 |

**Figure 6.1.1. Establishment and validation of the radioresistant EAC cell line model.** (A) The schematic diagram of the radioresistant model establishment. (B, D) Colony formation assay was performed to check the survival curves of OE33P and OE33R. Means ± SD, N = 3. Statistical comparisons were made using a paired two-tailed Student's t-test; *P < 0.05, **P < 0.01, ***P < 0.001. (C) The single-hit multi-target model was applied to this model. $D_0$ and $D_q$ values were calculated. $D_0$ is the "mean lethal dose", the dose on the straight-line portion of the survival curve to decrease the survival to 37%. $D_q$ is the quasi-threshold dose, is the width of the "shoulder," and correlates with repair capacity. (E) The volcano map shows the differentially expressed genes between OE33P and OE33R by the result of RNA-seq data. |logFC| > 2, log10 (adj.P.Value) > 2. (F) The major differentially expressed genes were exhibited in the heatmap. (G) AKR1C3 mRNA relative expression level in OE33P and OE33R was measured by qRT-PCR analysis. Mean ± SD, N = 3. (H) AKR1C3 protein expression level in OE33P and OE33R was validated by Western blot.

## 6.2. AKR1C3 could enhance the radioresistance in EAC cells

### 6.2.1. AKR1C3 improves colonies survival fraction after irradiation

Our group has already successfully established the AKR1C3 knockdown and overexpressing EAC cell line models by short-hairpin RNA, and relevant functional experiments have also been validated, such as cell proliferation assay and wound healing assay [93]. To better explore the mechanism of AKR1C3 and radioresistance in EAC cells, we chose OE33 VEC / OE33 AKR1C3 as the overexpressing model, and SKGT-4 shNC / SKGT-4 shAKR1C3 as the knockdown model for the further experiments. We performed Western blot to validate the transfection effect again, the results showed the knockdown and overexpression effect worked well (Figure 6.2.1. A). In the colony formation assay, OE33 AKR1C3 had a higher survival rate than OE33 VEC at 4 Gy and 6 Gy, while SKGT-4 shAKR1C3 had a lower survival rate than SKGT-4 shNC at 2 Gy, 4 Gy and 6 Gy (Figure 6.2.1. B, C). In order to avoid the colonies of SKGT-4 shAKR1C3 from being too less after 6 Gy, the cell seeding number in SKGT-4 shAKR1C3 was twice of that in SKGT-4 shNC.

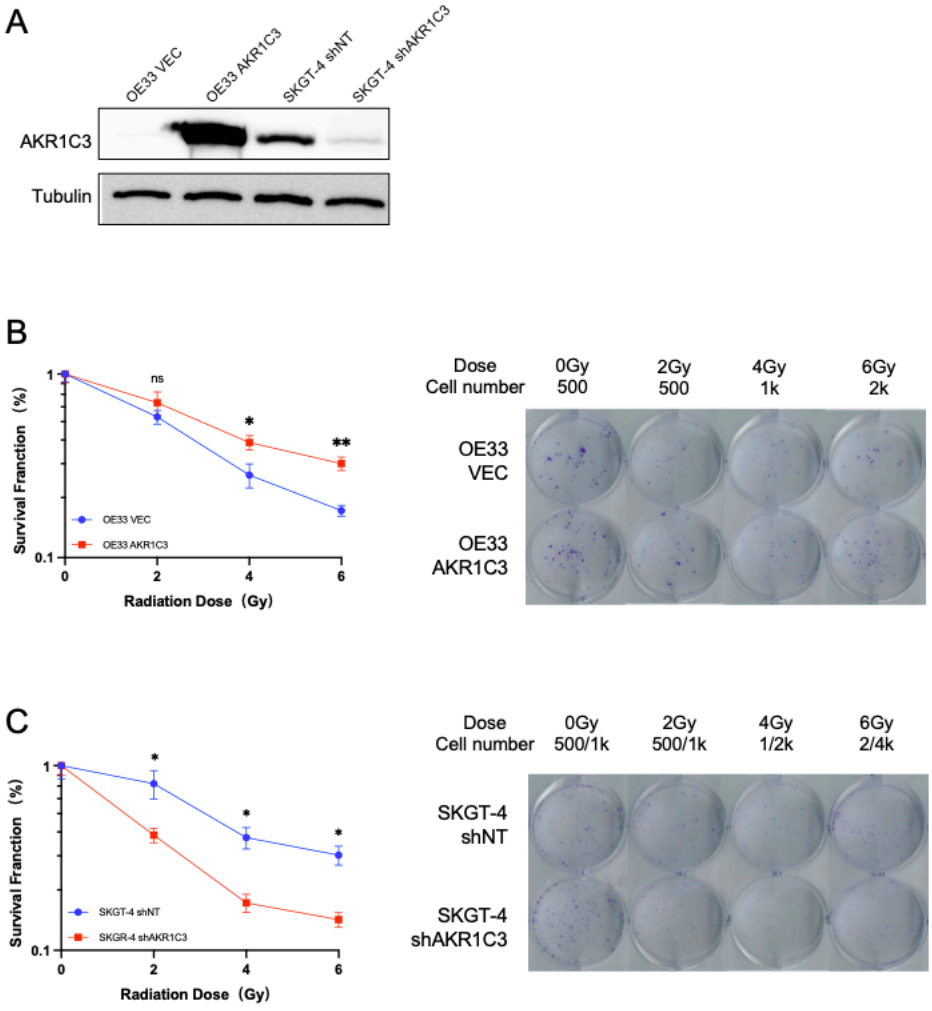


**Figure 6.2.1. AKR1C3 could enhance the radioresistance in EAC cells**

(A) Validation of stable overexpression of AKR1C3 in OE33 and knockdown of AKR1C3 in SKGT-4 by Western blot. (B, C) Survival fraction after 0 - 6 Gy irradiation in OE33 VEC / OE33 AKR1C3 and SKGT-4 shNC / SKGT-4 shAKR1C3. Data are presented as mean ± SD, N = 3, ns = no significant difference, * $p < 0.05$, ** $p < 0.01$.

### 6.2.2. AKR1C3 regulates the irradiation-induced apoptosis in EAC cells

To further characterize the role of AKR1C3 in the radioresistance of EAC, apoptosis assay was performed under flow cytometry. Annexin V and DAPI were selected as staining to identify the early and late apoptotic cells. The data showed there was no significant difference neither between OE33 VEC / OE33 AKR1C3 nor SKGT-4 shNC / SKGT-4 shAKR1C3 before irradiation. While 48h after 6 Gy irradiation, OE33 AKR1C3 had remarkably fewer apoptotic cells than OE33 VEC (Figure 6.2.2. A, B). On the contrary, 48h after 10 Gy irradiation, SKGT-4 shAKR1C3 had more apoptotic cells than SKGT-4 shNC (Figure 6.2.2. C, D).

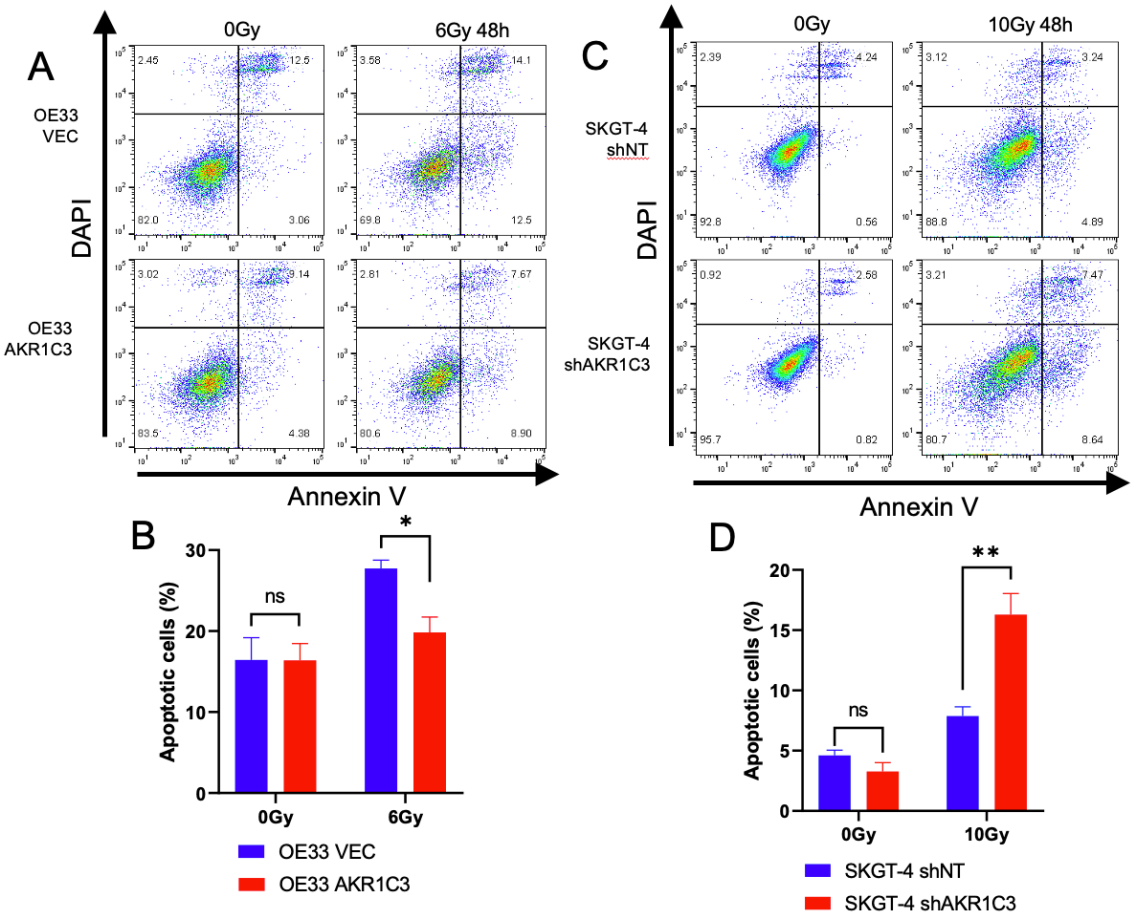


**Figure 6.2.2. AKR1C3 could regulate the irradiation-induced apoptosis in EAC cells**

(A, C) Cells were treated with 0 - 10 Gy gamma-ray irradiation. Flow cytometry was performed 48h after treatment. Dot plots showed the early and late apoptotic cells before or after irradiation in OE33 VEC / OE33 AKR1C3 and SKGT-4 shNC / SKGT-4 shAKR1C3 by Annexin V and DAPI staining. (B, D) Bar charts showed the percentage

of apoptotic cells in different groups. Data was presented as mean ± SD, N = 3, ns = no significant difference, * $p < 0.05$, ** $p < 0.01$.

### 6.3. AKR1C3 reduces the DNA damage after irradiation in EAC cells

To verify whether AKR1C3 is related to DNA damage after radiotherapy, we performed comet assay and immunofluorescence.

Comet assay, also known as the single-cell gel electrophoresis assay, is a simple and sensitive technique to detect DNA damage at single-cell level [149]. When the damaged DNA migrates through the electrophoresis gel, the "tail" looks like a comet passing by. The longer and thicker tails indicated more severe DNA damage. The percentage of Tail DNA had no significant difference between OE33 VEC / OE33 AKR1C3 or OE33P / OE33R before irradiation, while OE33 AKR1C3 and OE33R showed shorter DNA tails than OE33 VEC and OE33P after 6 Gy irradiation (Figure 6.3. A). It means OE33 AKR1C3 and OE33R had less DNA damage after irradiation compared to OE33 VEC and OE33P. In addition, SKGT-4 shAKR1C3 presented significantly longer DNA tails than SKGT-4 shNT after 10 Gy irradiation. However, we found SKGT-4 shAKR1C3 also had a higher percentage of Tail DNA before irradiation, this may be related to the knockdown effect.

γH2AX is a sensitive molecular marker of DNA damage and repair widely used for cancer and aging research [150-152]. Phosphorylation of H2AX is an early response to double-strand breaks. We treated cells with 3 - 8 Gy irradiation, and then fix after 30min. DAPI was stained for localizing the nucleus. The nuclear γH2AX foci were recorded and the fold change was calculated. OE33 AKR1C3 and OE33R presented lower fold change of nuclear γH2AX foci than OE33 VEC and OE33P ($P < 0.001$ and $P < 0.01$, respectively), suggesting less DNA damage after irradiation. While SKGT-4 shAKR1C3 showed a higher fold change of nuclear γH2AX foci than SKGT-4 shNC after irradiation ($P < 0.05$), suggesting more DNA damage after irradiation (Figure 6.3. B).

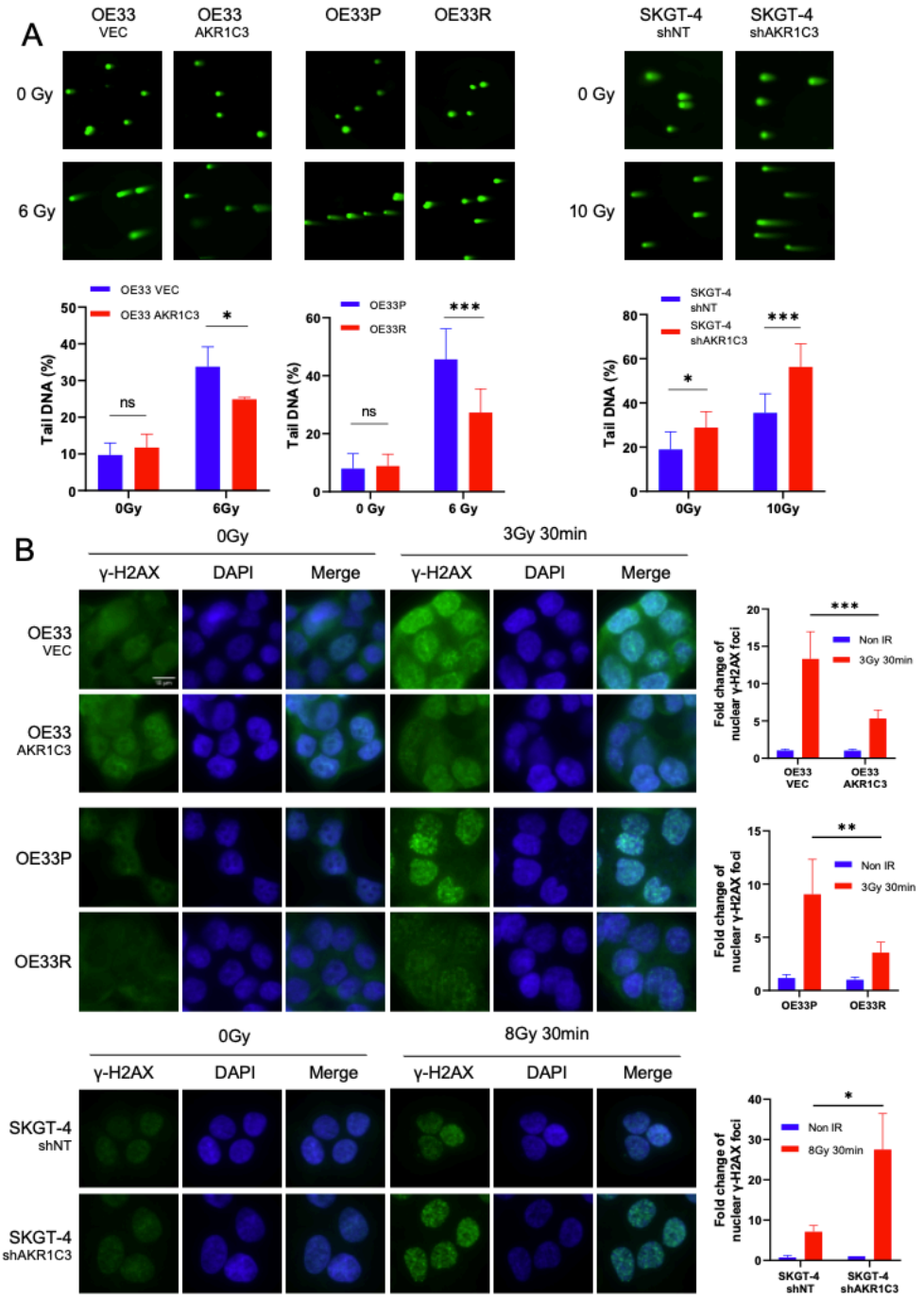


**Figure 6.3. AKR1C3 reduces the DNA damage after irradiation in EAC cells**

(A) Cells were treated with irradiation (6 Gy for OE33 and 10 Gy for SKGT-4). 4h after irradiation, cells were harvested and then electrophoresed. Nuclei were stained by Nancy-520 (Cat#01494, Sigma, Germany). Bar charts presented the percentage of Tail DNA in each group.

(B) Cells were treated with irradiation (3 Gy for OE33 and 8 Gy for SKGT-4). The fold change of the nuclear γH2AX foci was presented in the bar charts. Mean ± SD, three independent experiments, * $p < 0.05$, ** $p < 0.01$, *** $p < 0.001$, ns: no significant difference, $p > 0.05$.

## 6.4. AKR1C3 influences the mitochondrial function in EAC cells

### 6.4.1. Mitochondrial morphology alters in the radioresistant model

To better understand the changing of mitochondrial function after radiotherapy, we first explored the morphological feature of the radioresistant model by transmission electron microscope. OE33P and OE33R were fixed 24h after 2.5 Gy irradiation, the control groups didn't get treatment. We observed the distinctive morphological change in OE33P after radiotherapy, which appeared to have a more condensed membrane and more elongated mitochondrial characteristic (Figure 6.4. A), consistent with the typical ferroptosis morphology [108]. While OE33R already had this morphological change before radiotherapy, which we considered to be related to its long-term low-dose radiotherapy. After radiotherapy again, OE33R morphology did not alter significantly, which seemed to imply that it had become resistant to this external stimulus.

### 6.4.2. AKR1C3 regulates mitochondrial metabolism in EAC cells

To validate whether AKR1C3 can regulate mitochondrial metabolism, we performed Seahorse XF cell mito stress test and Seahorse XF glycolytic rate assay to measure oxygen consumption rate (OCR) and extracellular acidification rate (ECAR), respectively. OE33 AKR1C3 showed more obvious OCR changes after radiotherapy than OE33 VEC, for the ECAR part, the change between the two cell lines was about the same (Figure 6.4. B). SKGT-4 shNC also had higher OCR and ECAR changes than SKGT-4 shAKR1C3 after radiotherapy (Figure 6.4. C). OE33R had both higher OCR and ECAR after radiotherapy, while neither OCR nor ECAR of OE33P changed significantly (Figure 6.4. D).

### 6.4.3. AKR1C3 regulates mitochondrial activity after radiotherapy in EAC cells

Tetramethyl rhodamine ethyl ester (TMRE), a cell-permeant, cationic, red-orange fluorescent dye, is widely used for labeling active mitochondria. We stained knockdown and overexpressing cell lines before and after radiotherapy with TMRE and found that the median fluorescence intensity (MFI) was upregulated in OE33 AKR1C3 while downregulated in SKGT-4 shAKR1C3 after radiotherapy (Figure 6.4. E, F), suggesting AKR1C3 regulate mitochondrial activity in EAC cells.

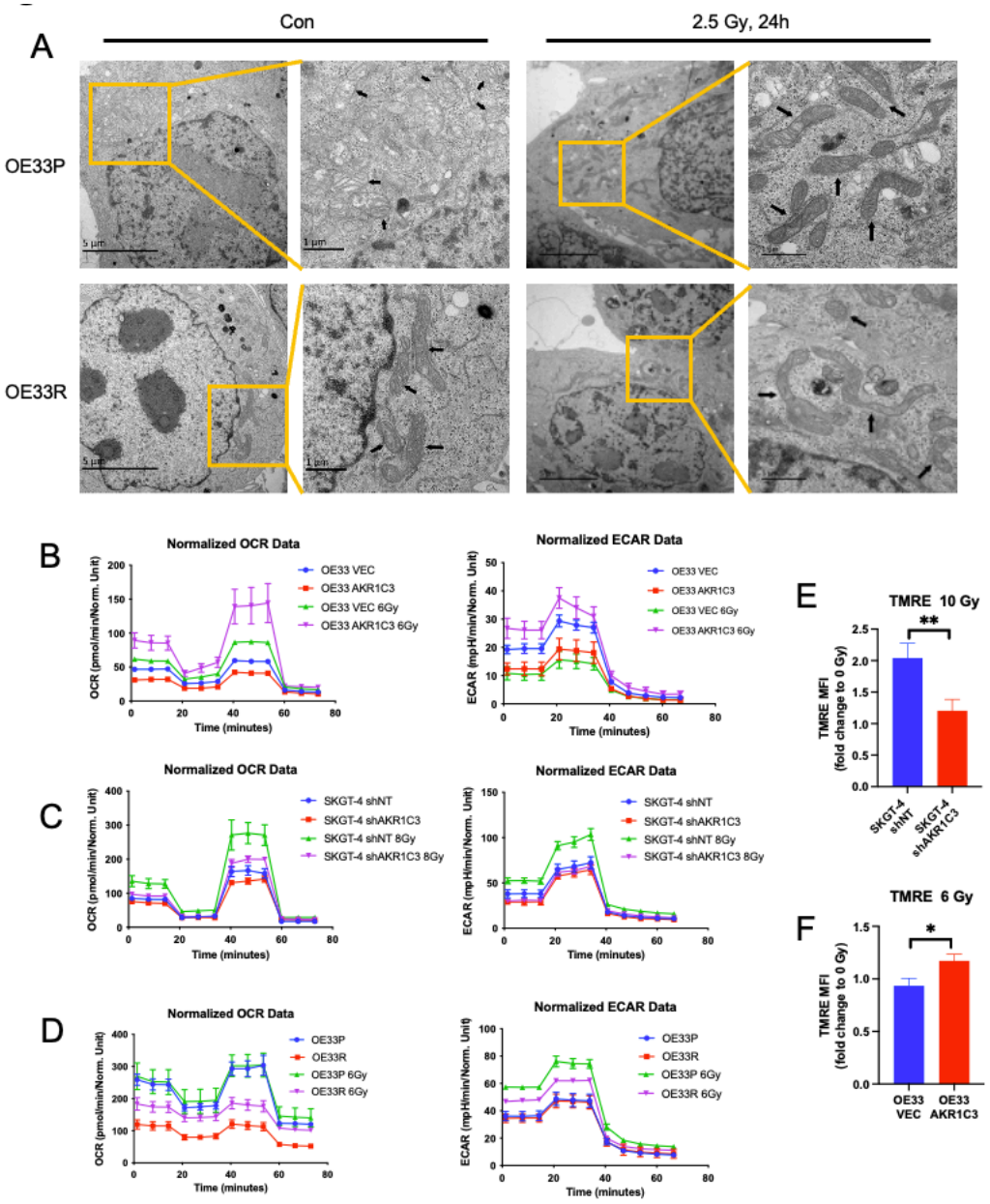


**Figure 6.4. AKR1C3 influences the mitochondrial function in EAC cells.**
(A) Transmission electron microscopy images of OE33P / OE33R before and after radiotherapy (2.5 Gy, fixation after 24h). Black arrow: mitochondria. A minimum of five cells in each group were examined. (B, C, D) Agilent Seahorse XF showed the corresponding OCR and ECAR. In the cell mito stress test, Oligomycin (at 20 minutes), FCCP (at 40 minutes), and Rotenone & Antimycin A (at 60 minutes) were added to the reaction separately. In the glycolytic rate assay, Rotenone & Antimycin A (at 20 minutes) and 2-deoxy-D-glucose (at 40 minutes) were added to the reaction separately. Mean ± SD, n = 5. (E, F) TMRE was stained for detecting mitochondrial activity. Bar charts showed the fold change of the TMRE MFI before and after radiotherapy. * $p < 0.05$, ** $p < 0.01$.

## 6.5. AKR1C3 inhibits irradiation-induced ferroptosis in EAC cells

### 6.5.1. AKR1C3 is closely related to ferroptosis

To further explore the mechanism between AKR1C3 and radioresistance, we performed KEGG pathway analysis based on our RNA-sequencing data. We found that some classic cellular pathways were enriched, such as: Notch, NF-kappa B and Wnt signaling pathways.

At the same time, we also found 7 of the 41 ferroptosis-associated genes were enriched from the DEGs of OE33P / OE33R which caught our attention (Figure 6.5.1. A). Our previous research found AKR1C3 could regulate GSH levels which was a critical antioxidant to detoxify ROS in cells [93]. Next, we merged the 238 ferroptosis suppressors from FerrDb2 database with the DEGs of OE33P / OE33R, five genes (AKR1C3, AKR1C2, AKR1C3, ADAMTS13 and PANX2) were found (Figure 6.5.1. B). We examined the SLC7A11 and GPX4 protein level in our cell lines, we found both of them were upregulated in OE33 ARK1C3 and OE33R compared to OE33 VEC and OE33P, while downregulated in SKGT-4 shAKR1C3 compared to SKGT-4 shNC (Figure 6.5.1. C). Furthermore, based on GEPIA database, we found AKR1C3 was positively correlated with SLC7A11 and GPX4 (Figure 6.5.1. D, E). The above data suggested that AKR1C3 is closely associated with ferroptosis in EAC cells. Unfortunately, through the Co-IP assay, we did not find a binding interaction between AKR1C3 and SLC7A11 / GPX4 (Figure 6.5.1. F). So far, no literature has reported the direct interaction between AKR1C3 and SLC7A11. There may be an indirect regulatory mechanism, which is worthy of our further exploration.

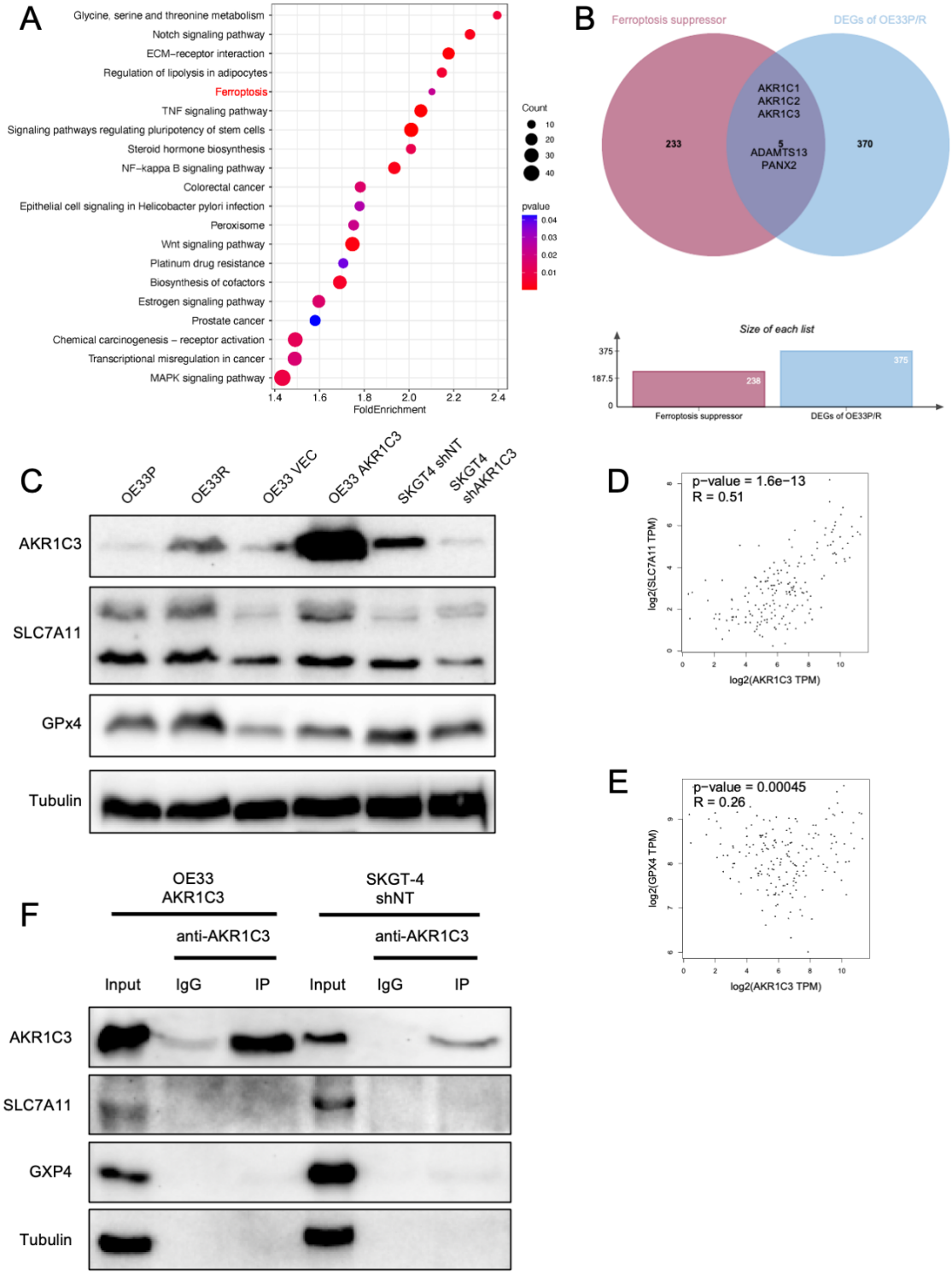


**Figure 6.5.1. AKR1C3 is closely related to ferroptosis in EAC cell lines.**
(A) Top 20 KEGG pathways ranked by fold enrichment were analyzed based on the DEGs of OE33P / OE33R. (B) Venn diagram analysis presented the five overlapped genes merged by 238 ferroptosis suppressors and 375 DEGs of OE33P / OE33R. (C) Representative immunoblot of the indicated proteins in OE33P / OE33R, OE33 VEC / OE33 AKR1C3 and SKGT-4 shNC / SKGT-4 shAKR1C3. (D, E) The correlation between AKR1C3 and SLC7A11 (D), AKR1C3 and GPX4 (E) was shown, analysis was

done in GEPIA based on TCGA database. (F). The interaction between AKR1C3 and SLC7A11 / GPX4 was validated by an endogenous Co-IP assay in OE33 AKR1C3 and SKGT-4 shNT cells. The input group served as a positive control, and IgG served as a negative control.

### 6.5.2. AKR1C3 suppresses erastin-induced ferroptosis in EAC cells

To continue to explore how AKR1C3 regulates ferroptosis, we first selected ferroptosis inducer erastin to treat our cell lines. We performed MTT assay to examine the sensitivity of erastin, the results showed the IC50 of erastin was significantly higher in OE33R and OE33 AKR1C3 than in OE33P and OE33 VEC, while lower in SKGT-4 shAKR1C3 than in SKGT-4 shNC, suggesting AKR1C3 would lead to erastin resistance in EAC cells (Figure 6.5.2. A). Next, we chose C11-Bodipy staining on flow cytometry to check the lipid peroxidation level, the fold change of the median fluorescence intensity (MFI) was calculated as: $\frac{\text{MFI of the erastin group}}{\text{MFI of the corresponding DMSO group}}$. The fold change of MFI in OE33R and OE33 AKR1C3 was lower than in OE33P and OE33 AKR1C3, while the fold change of MFI in SKGT-4 shAKR1C3 was higher than in SKGT-4 shNC (Figure 6.5.2. B). This indicated AKR1C3 could prevent cells from lipid peroxidation which further caused ferroptosis after erastin treatment.

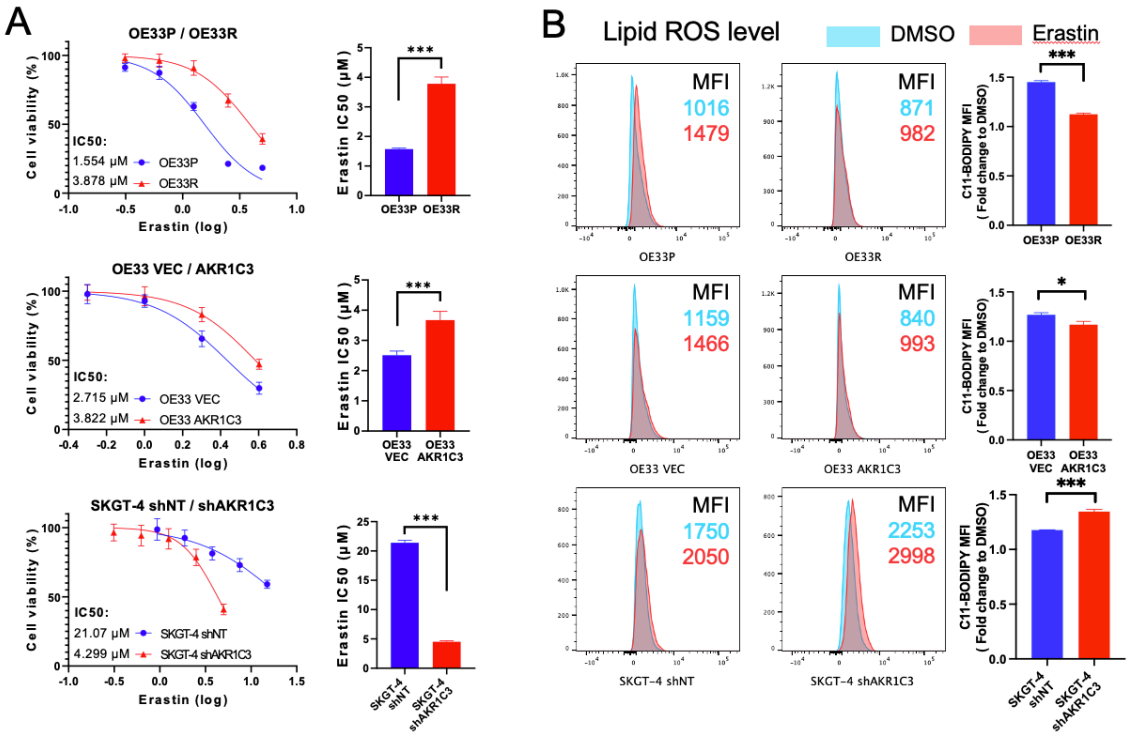


**Figure 6.5.2. AKR1C3 suppresses erastin-induced ferroptosis in EAC cells.** (A) OE33P / R, OE33 VEC / AKR1C3 and SKGT-4 shNT / shAKR1C3 cells were treated with 0.315 - 5 μM, 0.25 - 5 μM and 1.25 - 20 μM erastin respectively for 72h. The relative cell viability was measured by the MTT assay. (B) Lipid peroxidation level was detected

by C11-Bodipy staining on flow cytometry. The concentration of C11-Bodipy for staining was 1 μM. OE33 and SKGT-4 cells were treated with 1 μM and 2 μM erastin for 48h, respectively. Bar graphs showing erastin-induced relative fold change of lipid peroxidation levels. Minimum of ten thousand cells were recorded. Data was shown as mean ± SD of at least triplicates. * $p < 0.05$, ** $p < 0.01$, *** $p < 0.001$.

### 6.5.3. AKR1C3 inhibits the irradiation-induced ferroptosis in EAC cells

In order to verify whether AKR1C3 can inhibit irradiation-induced ferroptosis, we continued to detect C11-Bodipy level after radiotherapy. OE33P and OE33R had the slightly different MFI level before irradiation (891.67±6.51 vs 1,069.67±10.26), while after irradiation MFI was much higher in OE33P than in OE33R (1,733.67±20.84 vs 1,226.00±15.59). OE33 VEC and OE33 AKR1C3 had the similar trend, MFI was similar before irradiation (1,049.33±14.57 vs 1,085.33±28.02), while OE33 VEC had higher MFI than OE33 AKR1C3 after irradiation (1,896.67±20.21 vs 1,346.00±12.12). The MFI of SKGT-4 shNC was lower than that of SKGT-4 shAKR1C3 before irradiation (1,590.00±15.13 vs 2,462.00±31.00), but the difference of MFI between them was further exaggerated after radiotherapy (2,083.00±20.22 vs 4,377.67±42.10). We found the fold change of MFI was lower in OE33R and OE33 AKR1C3 but higher in SKGT-4 shAKR1C3 than in OE33P, OE33 VEC and SKGT-4 shNC respectively after radiotherapy (Figure 6.5.3.). The experimental results had the same trend as the results of erastin-induced ferroptosis, suggesting AKR1C3 could also inhibit the irradiation-induced ferroptosis in EAC cells.

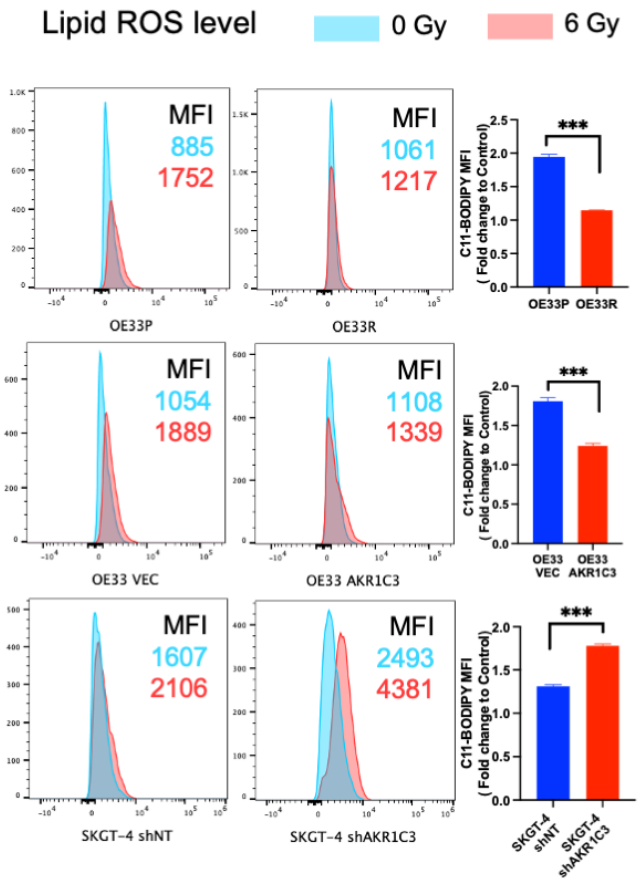


**Figure 6.5.3. AKR1C3 inhibits the irradiation induced ferroptosis in EAC cells.** OE33P / R, OE33 VEC / AKR1C3 and SKGT-4 shNT / shAKR1C3 cells were treated with 6 Gy. After 48h, lipid peroxidation level was detected by C11-Bodipy staining on flow cytometry. The concentration of C11-Bodipy for staining was 1 μM. Bar graphs showing irradiation-induced relative fold change of lipid peroxidation levels. Minimum of ten thousand cells were recorded. Data was shown as mean ± SD of at least triplicates. * $p < 0.05$, ** $p < 0.01$, *** $p < 0.001$.

## 6.6. AKR1C3 inhibitor could re-sensitize EAC cells to erastin.

### 6.6.1. Ferrostatin-1 (Ferr-1) could cause the radioresistance in AKR1C3 knockdown cells.

Ferrostatin-1 (Ferr-1), a synthetic antioxidant, acts as a classic hydroperoxyl radical scavenger which could suppress erastin-induced ferroptosis [153]. We first tested the effect of Ferr-1 in EAC cells. Z-VAD-FMK, a well-known apoptosis inhibitor, was also selected to test whether erastin-induced ferroptosis could be reversed. OE33 and SKGT-4 cells were treated with erastin, erastin + Ferr-1 or erastin + Z-VAD-FMK. Our results showed the cell viability of OE33P obviously decreased after erastin treatment; however, it recovered significantly after combination with Ferr-1; while in OE33R, Ferr-1 didn't

reverse the cell death caused by erastin. In the other two groups, Ferr-1 showed varying degrees of capacity to inhibit erastin-induced cell death (Figure 6.6.1. A). Interestingly, like in OE33P / R, Ferr-1 exhibited weaker “repair capacity” for cells with higher AKR1C3 expression level, but stronger “repair capacity” for cells with lower AKR1C3 expression level. At the same time, we also found that Z-VAD-FMK could not rescue erastin-induced cell death in all of our EAC cells.

The data mentioned above showed AKR1C3 could lead to radioresistance, and could also regulate irradiation induced-ferroptosis. Next step, we tried to demonstrate whether AKR1C3-induced radioresistance was due to ferroptosis inhibition. We performed colony formation assay, treated cells with 1 Gy irradiation, the 2$^{nd}$ day Ferr-1 or DMSO was added. The relative survival fraction presented the rescue effect of Ferr-1 in OE33P, OE33 VEC and SKGT-4 shAKR1C3 was more obvious than in OE33R, OE33 AKR1C3 and SKGT-4 shNC (Figure 6.6.1. B). The results indicated Ferr-1 could lead to cell survival after radiotherapy, and this effect was more obvious in lower AKR1C3 expressed cells.

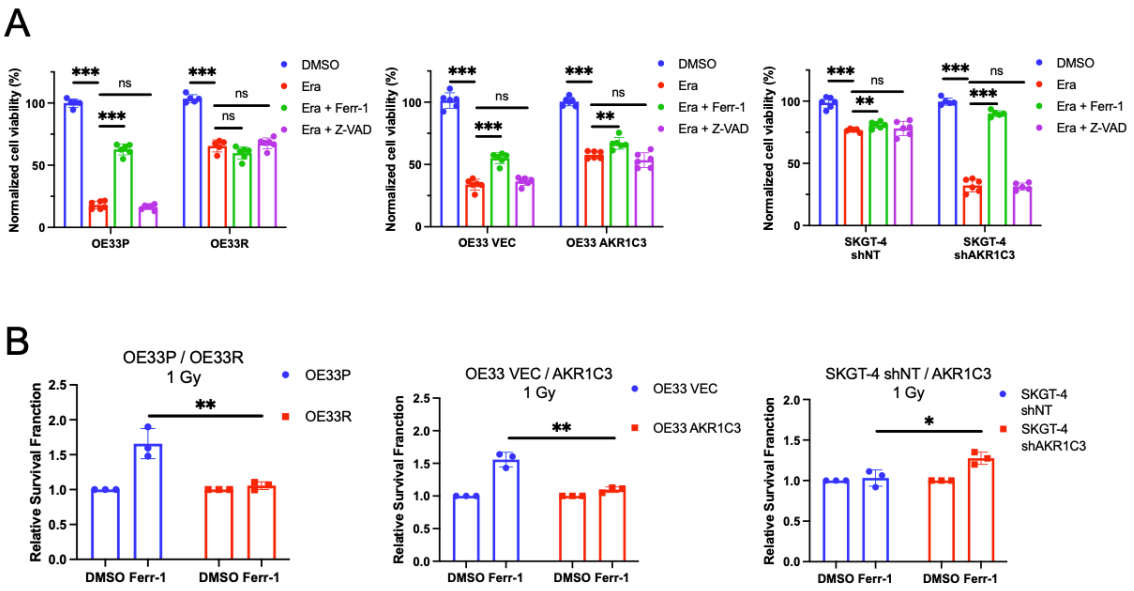


**Figure 6.6.1. AKR1C3 inhibits the irradiation-induced ferroptosis in EAC cells.** (A) OE33P / R, OE33 VEC / AKR1C3 and SKGT-4 shNT / shAKR1C3 cells were treated with erastin (2 μM, 2 μM and 5 μM respectively) for 72h, with 5 μM Ferr-1 for 48h, with Z-VAD-FMK 5 μM for 48h. The relative cell viability was measured by the MTT assay. Data was normalized with the DMSO groups. (B) 500 cells were seeded in the 6-well plated, 1 Gy irradiation after 24h, the concentration of Ferr-1 was 0.3μM. Cells were fixed and counted after 7-12 days. Data was shown as mean ± SD of at least triplicates. * $p < 0.05$, ** $p < 0.01$, *** $p < 0.001$. ns: no significant difference, $p > 0.05$.

### 6.6.2. AKR1C3 inhibitor could re-sensitize EAC cells to erastin

Our data has previously demonstrated that AKR1C3 can inhibit erastin-induced ferroptosis and cause erastin resistance. We wondered whether the AKR1C3 inhibitor

could rescue this resistance and re-sensitize cells to erastin. Medroxyprogesterone acetate (MPA), a hormonal medication of the progestin type, was reported as a selective inhibitor to suppress the enzyme activity of AKR1C3 [105]. We first tested the cytotoxicity of MPA by MTT assay, we found MPA had almost no damage on cells within 15 μM (Figure 6.6.2. A, B, C). We further checked the AKR1C3 expression level by Western blot with MPA treatment. The AKR1C3 protein level didn't change with 1-10 μM MPA treatment after 72h (Figure 6.6.2. B). Then, we performed an MTT assay to check the cell viability after treatment with erastin alone, MPA alone or erastin plus MPA. We found that the combined use of erastin and MPA resulted in a significant decrease in cell viability than using erastin alone (Figure 6.6.2. C, D, E). It indicated the inhibition of AKR1C3 could sensitize EAC cells to erastin in EAC cells.

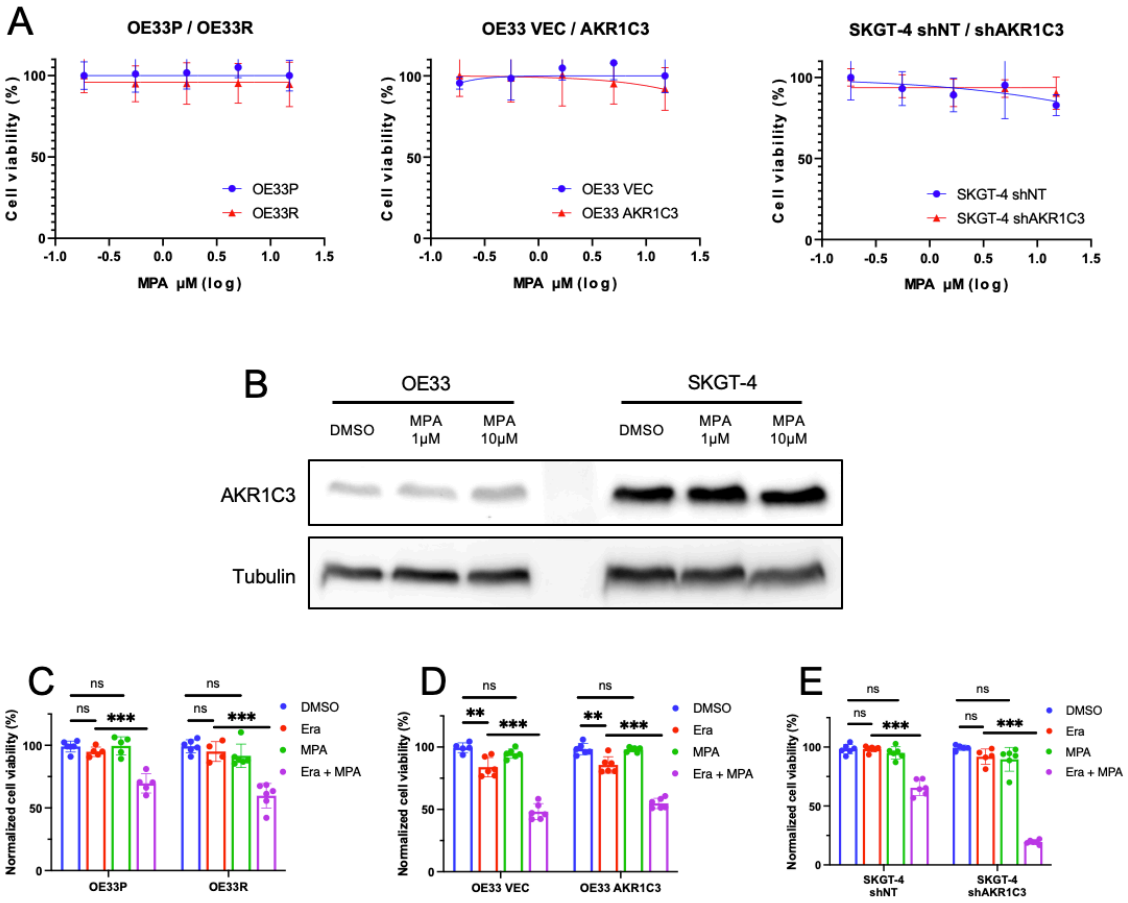


**Figure 6.6.2. AKR1C3 inhibitor re-sensitizes EAC cells to earstin**

(A) OE33P / R, OE33 VEC / AKR1C3 and SKGT-4 shNT / shAKR1C3 cells were treated with MPA (up to 15 μM) for 72h. The relative cell viability was measured by the MTT assay. Data was normalized with the DMSO groups. Mean ± SD of five replicates, three independent experiments performed. (B) OE33 and SKGT-4 cells were treated with 1 and 10 μM MPA for 72h. DMSO set as a control. Protein level was measured by Western blot. (C, D, E) OE33P / R, OE33 VEC / AKR1C3 and SKGT-4 shNT / shAKR1C3 cells were treated with erastin (1, 1.5 and 1.5 μM respectively), 10 μM MPA

and combined use of erastin / MPA for 48h. The relative cell viability was measured by the MTT assay. Data was normalized with the DMSO groups. Mean ± SD of five replicates, three independent experiments performed. * $p < 0.05$, ** $p < 0.01$, *** $p < 0.001$. ns: no significant difference, $p > 0.05$.

## 6.7. AKR1C3 mRNA expression level was upregulated in esophageal cancer and related to poor prognosis

We previously found AKR1C3 expression level was regulated in EAC from GSE26886 and GSE92396 [93]. Additionally, from TCGA database, we could also find AKR1C3 expression was upregulated in esophageal cancer which included both EAC and ESCC (Figure 6.7. A). The survival curve showed the median survival time was 23.1 months in the high AKR1C3 group and 27.1 months in the low AKR1C3 group revealing that high AKR1C3 expression would confer the poor prognosis in EAC (Figure 6.7. B).

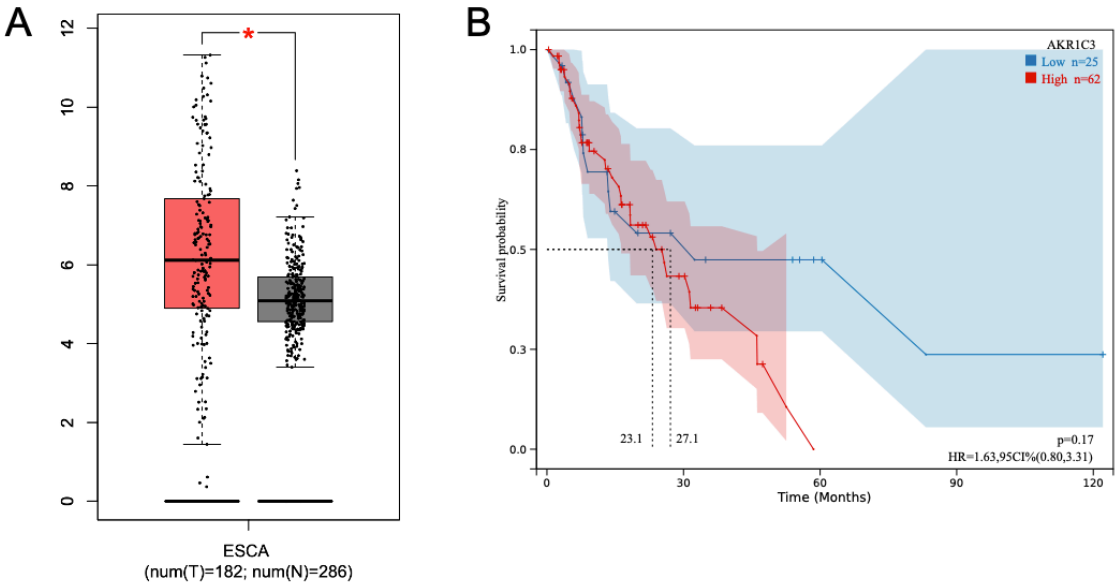


**Figure 6.7. AKR1C3 expression level was upregulated in esophageal cancer and related to poor prognosis**

(A) AKR1C3 expression level was higher in tumor tissue than in normal tissue in esophageal cancer. Data was from TCGA. Figure was composed with GEPIA. (B) Survival data of esophageal cancer was downloaded from TCGA, EAC subgroup was sorted. Kaplan-Meier survival analysis showed that higher AKR1C3 expression was associated with a trend of poor prognosis. Low AKR1C3 group number = 25, High AKR1C3 group number = 62. * $p < 0.05$.

# 7. DISCUSSION

Although the mounting multimodal approaches for cancer treatment is remarkable, the prognosis of EAC is still dismal. Therapy resistance including chemoresistance and radioresistance might be mainly responsible for the poor prognosis [2,154,155]. Our previous study revealed AKR1C3 could mediate chemoresistance via detoxification of ROS; on the other hand, growing evidence suggested AKR1C3 enhanced radioresistance in ESCC [97,106,156]. However, the radioresistant mechanism of AKR1C3 has not been deeply studied in EAC.

Xiong et al. [97] found AKR1C3 expression level was extremely higher in ESCC radioresistant cell lines - KY170 and TE13 and acted a vital role in oxidative stress. We wondered whether AKR1C3 functions similarly to ESCC in EAC, or whether there are other distinct phenotypes and mechanisms in EAC. The first dilemma in front of us was how to establish radioresistance cell line. Different EAC cell lines had different responses to irradiation, SKGT-4 and OE19 were relatively less responsive, while OE33 was relatively more sensitive to irradiation. Finally, we successfully established OE33 as a radioresistance model according to Dr. Maher's suggestion [45]. Our work validated OE33 radioresistant cell line (OE33R) has more survival fraction than OE33 parental cell line (OE33P). The RNA-seq data revealed AKR1C3 was obviously upregulated in OE33R, which was consistent with the radioresistant model in ESCC [97]. We confirmed AKR1C3 expression level again both in protein and mRNA levels, the results were consistent. In addition, besides AKR1C3, AKR family including AKR1C1, AKR1C2 and AKR1C4 was also upregulated in OE33R, suggesting AKR family played a critical role in the modulation of radioresistance. Interestingly, the ferroptosis-associated genes, such as FSP1, IRP1, IRP2 and SLC7A11 exhibited significantly differential expression in OE33P/OE33R. Mounting studies have found AKR1C3 was a potential ferroptosis-related biomarker in prostate cancer, thyroid cancer, kidney renal papillary cell carcinoma, chronic lymphocytic leukemia, colon adenocarcinoma and HCC [157-162]. Furthermore, AKR1C3 was recently reported to inhibit ferroptosis in HCC via YAP/SLC7A11 signaling pathway [163]. Exploring the function of AKR1C3 in IR-induced ferroptosis might be a meaningful attempt.

Irradiation is able to release electrons to generate high-energy damage to induce DNA double strands breaks (DSBs), but it can also generate ROS to cause DNA damage through water radiolysis [164]. We demonstrated AKR1C3 could enhance the radioresistance in our overexpressing and knockdown cell lines. On the other hand, AKR1C3 also reduced DNA damage after irradiation. Flow cytometry analysis exhibited

that AKR1C3 inhibited IR-induced apoptosis. This might be due to the regulation of ROS by AKR1C3. Our previous study has already confirmed AKR1C3 could reduce intracellular ROS levels in EAC cells, which partly explained the effect of ARK1C3 on IR-induced DNA damage and apoptosis. While the total ROS level is not enough to support the effect of AKR1C3 on ferroptosis. To further validate the hypothesis, we performed TEM in our radioresistant model. OE33P showed more condensed and elongated mitochondrial changes after IR than before IR, which was consistent with the typical morphological changes of ferroptosis. While OE33R already showed condensed and elongated mitochondria before IR, and it didn't have obvious changes after IR. OE33R may have adapted to such long-term IR stimulation, and thus maintained its "defensive state". TMRE staining results showed AKR1C3 could mediate mitochondrial activity. To further explore the effect of AKRC13 on mitochondrial function, we checked OCR and ECAR levels by Seahorse assay. OE33 AKR1C3 and OE33R showed a higher degree of upregulation than OE33 VEC and OE33P, respectively in OCR level after IR. Similar trend was found in SKGT-4 shNT/AKR1C3, SKGT-4 shNT had a higher upregulation than SKGT-4 shAKR1C3 in OCR level. C11-Bodipy, a sensitively fluorescent radio-probe for detecting lipid peroxidation in living cells, has been wildly used in ferroptosis-related research [165]. Our C11-Bodipy staining exhibited AKR1C3 could reduce the lipid peroxidation after IR or ferroptosis inducer-erastin [166], further demonstrating AKR1C3 could regulate ferroptosis. We also found ferroptosis associated pathway was enriched in our RNA-seq data by KEGG pathway analysis. SLC7A11 and GPX4 are two critical proteins to regulate ferroptosis through the canonical SLC7A11/GSH/GPX4 pathway [167]. We found SLC7A11 and GPX4 protein level was upregulated in OE33 AKR1C3 and OE33R, while downregulated in SKGT-4 shAKR1C3. Furthermore, GEPIA database showed a positive correlation between AKR1C3 / SLC7A11 and AKR1C3 / GPX4 [168]. However, the result of the co-IP assay didn't detect the direct binding interaction in AKR1C3 and SLC7A11 / GPX4. We speculated that AKR1C3 might regulate SLC7A11 or GPX4 through some other mechanisms which need to be further explored.

The suppressor of cytokine signaling 2 (SOCS2) was found to have direct interaction with SLC7A11 in HCC cells by co-IP assay, acting as a bridge to transfer ubiquitin to SLC7A11, further causing the polyubiquitination degradation of SLC7A11; this finding indicated SOCS2 could regulate ferroptosis and sensitize HCC cells to irradiation [169]. Another study showed the binding interaction between SLC7A11 and NEDD4L was enhanced after irradiation by co-IP assay in breast cancer cells, and NEDD4L knockdown could significantly decrease the ubiquitination of SLC7A11 [170]. P53 was also found to play a critical role in ferroptosis, it could repress the transcription of SLC7A11, further block the cystine uptake, eventually cause ferroptosis [171]. P53-mediated

suppression of SLC7A11 could lead to the activation of arachidonate 12-lipoxygenase (ALOX12), resulting ROS stress and ferroptosis, it is worth mentioning that the p53-ALOX12 axis was independent of GPX4 [172]. CAMP response element-binding protein (CREB), a transcription factor highly expressed in lung adenocarcinoma, could directly bind to CREB motif in the GPX4 promoter to inhibit ferroptosis [173]. In future studies, further exploring the interaction between AKR1C3 and the above genes may bring some new clues for ferroptosis.

Erastin is a highly effective ferroptosis inducer that can decrease GSH level by directly suppressing xCT system [135]. Erastin is involved in the RAS–RAF–MEK signaling pathway which regulates the basic cell functions such as proliferation, differentiation and survival [174,175]. Mitochondrial voltage-dependent anion channel is proven as a therapeutic target of erastin, knockdown of VDAC2 or VDAC3 could cause resistance to erastin [176]. Scott J Dixon et al. isolated five clonal cell lines from prostate cancer cells strongly resistant to erastin and then performed RNA-seq for these clonal cell lines versus the parental cell line. AKR1C3, as well as AKR1C1/AKR1C2, were significantly upregulated in the RNA-seq data, implicating AKR1C family might cause erastin-resistance by enhance the prevention of lipid peroxidation-induced destruction in plasma membrane during ferroptosis [177]. In our study, we demonstrated that AKR1C3 exhibited a robustly resistant capacity to erastin in EAC cells, which was consistent to the results mentioned above. Moreover, ferr-1, a ferroptosis inhibitor, was found to have a stronger capacity to rescue the cell death induced by erastin or IR in AKR1C3 low-expressed cells than in AKR1C3 high-expressed cells in our present study. Then, we performed MTT assays to check the cell viability by co-culture with erastin, MPA (an AKR1C3 inhibitor) and erastin + MPA. The result proved AKR1C3 inhibition would sensitize cells to erastin. So far, we have demonstrated AKR1C3 could inhibit IR-induced ferroptosis via SLC7A11/GSH/GPX4 pathway. While our previous study revealed AKR1C3 could mediate GSH level by regulating AKT/GSH pathway, implicating AKR1C3 affected GSH levels in multiple pathways (Figure 7.1.).

In addition to the canonical SLC7A11/GSH/GPX4 pathway, we also found that the mRNA level of FSP1 was significantly upregulated in OE33R from our RNA-seq data (Figure 5.5.1 F). As we mentioned before in the introduction part, FSP1 could reduce CoQ to $CoQH_2$ in the plasma membrane; $CoQH_2$ could detoxify lipid peroxidation as an antioxidant [120]. CoQ-FSP1 axis is an emerging ferroptosis pathway independent of GPX4, which has been extensively studied in recent years [139,178,179]. However, it is still unknown whether FSP1 may also mediate the radioresistance in EAC, maybe there are some unexplored direct or indirect interactions between FSP1 and AKR1C3. At the same time,

we will focus our future study on target treatment of AKR1C3 *in vivo*, to provide more valuable evidence for the clinical treatment of radioresistance.

So far, numerous studies showed AKR1C3 could be a potential biomarker for multiple cancers. Peraldo-Neia et al reported that inhibition of AKR1C3 could suppress cell proliferation and sensitize the chemotherapy in oropharynx squamous cell carcinoma (OPSCC), a subtype of HNSCC; additionally, AKR1C3 expression level in 111 independent OPSCC patients was positively correlated with a poor prognosis [180]. In addition, other studies indicated that AKR1C3 had a potential value in the clinical diagnosis of T acute lymphoblastic leukemia/lymphoma [181,182]. In prostate cancer, AKR1C3 expression was positively correlated with Gleason score, suggesting AKR1C3 could serve as a promising biomarker for the prognosis [183]. In our studies, we have validated AKR1C3 could both mediate chemoresistance and radioresistance in EAC cells, however, to consider AKR1C3 as a biomarker of EAC, we still need more clinical data support. In our further study, collecting more clinical evidence will be our main exploration goal.

In this study, we revealed that AKR1C3 plays a critical role in radioresistance of EAC. AKR1C3 could enhance radioresistance and potentially act as a promising biomarker and therapeutic target in radioresistant EAC patients. AKR1C3 could regulate ferroptosis through detoxification of lipid peroxidation, which is involved in the canonical SLC7A11/GSH/GPX4 signaling pathway. Combined with our previous study on AKR1C3 regulating chemotherapy resistance, we believe that AKR1C3 is a promising biomarker to predict and access adjuvant therapy. In the future, in vivo experiments and clinical trials targeting AKR1C3 might bring more therapeutic evidence for the adjuvant therapy of EAC.

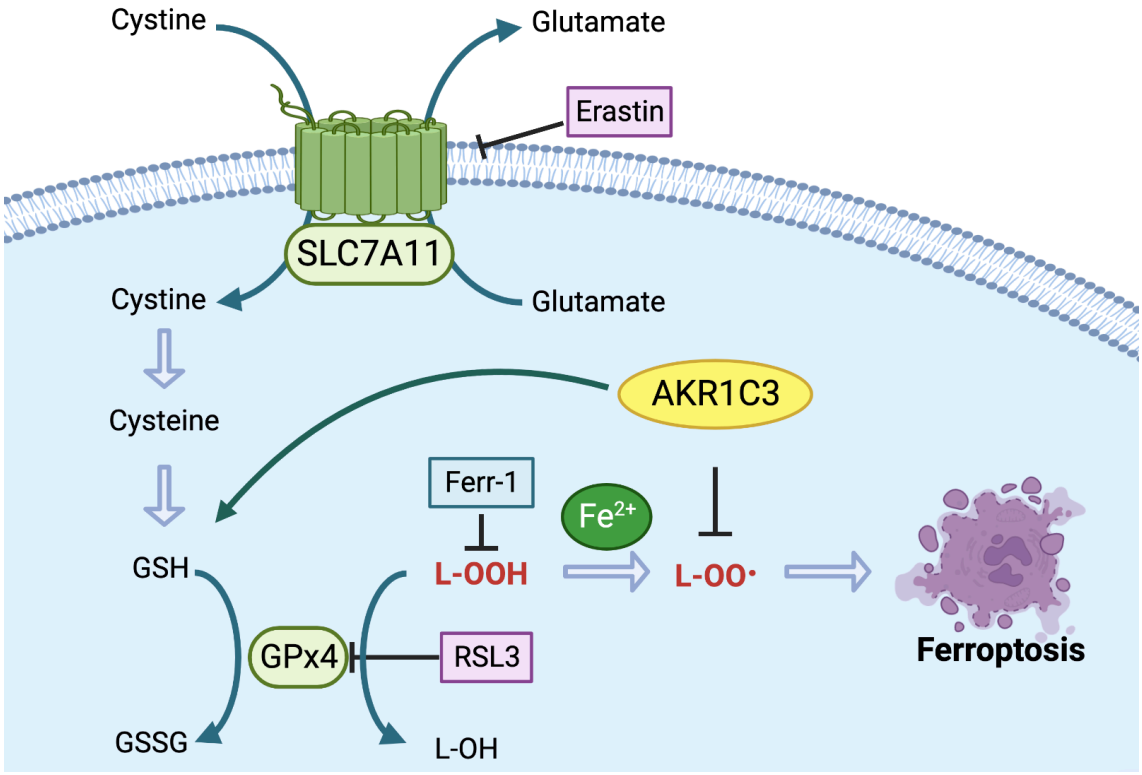


**Figure 7.1. The molecular mechanism of AKR1C3 mediating ferroptosis of EAC cells.**

AKR1C3 inhibits ferroptosis via regulation of SLC7A11/GSH/GPX4 signaling pathway. GSH is a critical antioxidant that undergoes redox reaction with phospholipid hydroperoxides (L-OOH) with the catalysis by GPX4. Overexpressing AKR1C3 could upregulate the expression of SLC7A11 and GPX4. Upregulated SLC7A11 provides more cystine for GSH synthesis. Moreover, upregulated GPX4 detoxifies more L-OOH through GSH-involved redox reaction. Radioresistance leads to AKR1C3 upregulation which significantly suppresses erastin-induced ferroptosis. Inhibition of AKR1C3 re-sensitizes EAC cells to erastin.

# 8. REFERENCE


1. Sung H, Ferlay J, Siegel RL, et al. Global Cancer Statistics 2020: GLOBOCAN Estimates of Incidence and Mortality Worldwide for 36 Cancers in 185 Countries. *CA: a Cancer Journal For Clinicians* 2021; **71**(3): 209-49.
2. Rogers JE, Sewastjanow-Silva M, Waters RE, Ajani JA. Esophageal cancer: emerging therapeutics. *Expert Opin Ther Targets* 2022; **26**(2): 107-17.
3. Joseph A, Raja S, Kamath S, et al. Esophageal adenocarcinoma: A dire need for early detection and treatment. *Cleve Clin J Med* 2022; **89**(5): 269-79.
4. Smyth EC, Lagergren J, Fitzgerald RC, et al. Oesophageal cancer. *Nat Rev Dis Primers* 2017; **3**: 17048.
5. Prabhu A, Obi KO, Rubenstein JH. The synergistic effects of alcohol and tobacco consumption on the risk of esophageal squamous cell carcinoma: a meta-analysis. *Am J Gastroenterol* 2014; **109**(6): 822-7.
6. Cooper SC, Day R, Brooks C, Livings C, Thomson CS, Trudgill NJ. The influence of deprivation and ethnicity on the incidence of esophageal cancer in England. *Cancer Causes Control* 2009; **20**(8): 1459-67.
7. DiSiena M, Perelman A, Birk J, Rezaizadeh H. Esophageal Cancer: An Updated Review. *South Med J* 2021; **114**(3): 161-8.
8. Arnold M, Laversanne M, Brown LM, Devesa SS, Bray F. Predicting the Future Burden of Esophageal Cancer by Histological Subtype: International Trends in Incidence up to 2030. *Am J Gastroenterol* 2017; **112**(8): 1247-55.
9. Domper Arnal MJ, Ferrández Arenas Á, Lanas Arbeloa Á. Esophageal cancer: Risk factors, screening and endoscopic treatment in Western and Eastern countries. *World J Gastroenterol* 2015; **21**(26): 7933-43.
10. Lagergren J, Lagergren P. Recent developments in esophageal adenocarcinoma. *CA: a Cancer Journal For Clinicians* 2013; **63**(4): 232-48.
11. Iriarte F, Su S, Petrov RV, Bakhos CT, Abbas AE. Surgical Management of Early Esophageal Cancer. *Surg Clin North Am* 2021; **101**(3): 427-41.
12. Koop H. Reflux disease and Barrett's esophagus. *Endoscopy* 2000; **32**(2): 101-7.
13. Rubenstein JH, Shaheen NJ. Epidemiology, Diagnosis, and Management of Esophageal Adenocarcinoma. *Gastroenterology* 2015; **149**(2).
14. Cooper GS, Kou TD, Chak A. Receipt of previous diagnoses and endoscopy and outcome from esophageal adenocarcinoma: a population-based study with temporal trends. *Am J Gastroenterol* 2009; **104**(6): 1356-62.
15. Verbeek RE, Leenders M, Ten Kate FJW, et al. Surveillance of Barrett's esophagus and mortality from esophageal adenocarcinoma: a population-based cohort study. *Am J Gastroenterol* 2014; **109**(8): 1215-22.
16. Wang J, Tang L, Lin L, Li Y, Li J, Ma W. Imaging characteristics of esophageal cancer in multi-slice spiral CT and barium meal radiography and their early diagnostic value. *J Gastrointest Oncol* 2022; **13**(1): 49-55.
17. Xia R, Zeng H, Liu W, et al. Estimated Cost-effectiveness of Endoscopic Screening for Upper Gastrointestinal Tract Cancer in High-Risk Areas in China. *JAMA Netw Open* 2021; **4**(8): e2121403.
18. Yang H, Hu B. Recent advances in early esophageal cancer: diagnosis and treatment based on endoscopy. *Postgrad Med* 2021; **133**(6): 665-73.
19. Watanabe M, Otake R, Kozuki R, et al. Recent progress in multidisciplinary treatment for patients with esophageal cancer. *Surg Today* 2020; **50**(1): 12-20.

20. Obermannová R, Alsina M, Cervantes A, et al. Oesophageal cancer: ESMO Clinical Practice Guideline for diagnosis, treatment and follow-up. *Ann Oncol* 2022; **33**(10).
21. Ishihara R, Arima M, Iizuka T, et al. Endoscopic submucosal dissection/endoscopic mucosal resection guidelines for esophageal cancer. *Dig Endosc* 2020; **32**(4): 452-93.
22. Mansour NM, Groth SS, Anandasabapathy S. Esophageal Adenocarcinoma: Screening, Surveillance, and Management. *Annu Rev Med* 2017; **68**: 213-27.
23. van Hagen P, Hulshof MCCM, van Lanschot JJB, et al. Preoperative chemoradiotherapy for esophageal or junctional cancer. *N Engl J Med* 2012; **366**(22): 2074-84.
24. Toxopeus E, van der Schaaf M, van Lanschot J, et al. Outcome of Patients Treated Within and Outside a Randomized Clinical Trial on Neoadjuvant Chemoradiotherapy Plus Surgery for Esophageal Cancer: Extrapolation of a Randomized Clinical Trial (CROSS). *Ann Surg Oncol* 2018; **25**(8): 2441-8.
25. von Holzen U, Schmidt S, Hayoz S, et al. Surgical Outcomes After Neoadjuvant Chemoradiation Followed by Curative Surgery in Patients With Esophageal Cancer: An Intergroup Phase III Trial of the Swiss Group for Clinical Cancer Research (SAKK 75/08). *Ann Surg* 2022; **275**(6): 1130-6.
26. Banks KC, Hsu DS, Velotta JB. Outcomes of Minimally Invasive and Robot-Assisted Esophagectomy for Esophageal Cancer. *Cancers (Basel)* 2022; **14**(15).
27. Shapiro J, van Lanschot JJB, Hulshof MCCM, et al. Neoadjuvant chemoradiotherapy plus surgery versus surgery alone for oesophageal or junctional cancer (CROSS): long-term results of a randomised controlled trial. *Lancet Oncol* 2015; **16**(9): 1090-8.
28. Ajani JA, D'Amico TA, Bentrem DJ, et al. Esophageal and Esophagogastric Junction Cancers, Version 2.2019, NCCN Clinical Practice Guidelines in Oncology. *J Natl Compr Canc Netw* 2019; **17**(7): 855-83.
29. Shah MA, Kennedy EB, Catenacci DV, et al. Treatment of Locally Advanced Esophageal Carcinoma: ASCO Guideline. *J Clin Oncol* 2020; **38**(23): 2677-94.
30. Kitagawa Y, Uno T, Oyama T, et al. Esophageal cancer practice guidelines 2017 edited by the Japan Esophageal Society: part 1. *Esophagus* 2019; **16**(1).
31. Fan N, Wang Z, Zhou C, et al. Comparison of outcomes between neoadjuvant chemoradiotherapy and neoadjuvant chemotherapy in patients with locally advanced esophageal cancer: A network meta-analysis. *EClinicalMedicine* 2021; **42**: 101183.
32. Yuan Z, Wang X, Geng X, et al. Liquid biopsy for esophageal cancer: Is detection of circulating cell-free DNA as a biomarker feasible? *Cancer Commun (Lond)* 2021; **41**(1): 3-15.
33. Zhou N, Hofstetter WL. Prognostic and therapeutic molecular markers in the clinical management of esophageal cancer. *Expert Rev Mol Diagn* 2020; **20**(4): 401-11.
34. Lagergren J, Smyth E, Cunningham D, Lagergren P. Oesophageal cancer. *Lancet* 2017; **390**(10110): 2383-96.
35. Mao C, Zeng X, Zhang C, et al. Mechanisms of Pharmaceutical Therapy and Drug Resistance in Esophageal Cancer. *Front Cell Dev Biol* 2021; **9**: 612451.
36. Ho ALK, Smyth EC. A global perspective on oesophageal cancer: two

diseases in one. *Lancet Gastroenterol Hepatol* 2020; **5**(6): 521-2.
37. Lohan-Codeço M, Barambo-Wagner ML, Nasciutti LE, Ribeiro Pinto LF, Meireles Da Costa N, Palumbo A. Molecular mechanisms associated with chemoresistance in esophageal cancer. *Cell Mol Life Sci* 2022; **79**(2): 116.
38. Vasan N, Baselga J, Hyman DM. A view on drug resistance in cancer. *Nature* 2019; **575**(7782): 299-309.
39. Stüben BO, Stuhlfelder J, Kemper M, et al. Completion of FLOT Therapy, Regardless of Tumor Regression, Significantly Improves Overall Survival in Patients with Esophageal Adenocarcinoma. *Cancers* 2022; **14**(4).
40. Zhou C, Wang Z, Li J, et al. Aldo-Keto Reductase 1C3 Mediates Chemotherapy Resistance in Esophageal Adenocarcinoma via ROS Detoxification. *Cancers* 2021; **13**(10).
41. Baskar R, Itahana K. Radiation therapy and cancer control in developing countries: Can we save more lives? *Int J Med Sci* 2017; **14**(1): 13-7.
42. Zhang H, Si J, Yue J, Ma S. The mechanisms and reversal strategies of tumor radioresistance in esophageal squamous cell carcinoma. *J Cancer Res Clin Oncol* 2021; **147**(5): 1275-86.
43. Tu Z, Xu B, Qu C, et al. BRCC3 acts as a prognostic marker in nasopharyngeal carcinoma patients treated with radiotherapy and mediates radiation resistance in vitro. *Radiat Oncol* 2015; **10**: 123.
44. Qu C, Zhao Y, Feng G, et al. RPA3 is a potential marker of prognosis and radioresistance for nasopharyngeal carcinoma. *J Cell Mol Med* 2017; **21**(11): 2872-83.
45. Lynam-Lennon N, Reynolds JV, Pidgeon GP, Lysaght J, Marignol L, Maher SG. Alterations in DNA repair efficiency are involved in the radioresistance of esophageal adenocarcinoma. *Radiat Res* 2010; **174**(6): 703-11.
46. Melsens E, De Vlieghere E, Descamps B, et al. Hypoxia imaging with 18F-FAZA PET/CT predicts radiotherapy response in esophageal adenocarcinoma xenografts. *Radiat Oncol* 2018; **13**(1): 39.
47. Chen D, Su H, Li Y, et al. miR-20b and miR-125a promote tumorigenesis in radioresistant esophageal carcinoma cells. *Aging (Albany NY)* 2021; **13**(7): 9566-81.
48. Wang J, Ma X, Si H, et al. Role of long non-coding RNA H19 in therapy resistance of digestive system cancers. *Mol Med* 2021; **27**(1): 1.
49. Donlon NE, Davern M, O'Connell F, et al. Impact of radiotherapy on the immune landscape in oesophageal adenocarcinoma. *World J Gastroenterol* 2022; **28**(21): 2302-19.
50. Smit JK, Faber H, Niemantsverdriet M, et al. Prediction of response to radiotherapy in the treatment of esophageal cancer using stem cell markers. *Radiother Oncol* 2013; **107**(3): 434-41.
51. Penning TM, Jonnalagadda S, Trippier PC, Rižner TL. Aldo-Keto Reductases and Cancer Drug Resistance. *Pharmacol Rev* 2021; **73**(3): 1150-71.
52. Hyndman D, Bauman DR, Heredia VV, Penning TM. The aldo-keto reductase superfamily homepage. *Chem Biol Interact* 2003; **143-144**: 621-31.
53. Jez JM, Penning TM. The aldo-keto reductase (AKR) superfamily: an update. *Chem Biol Interact* 2001; **130-132**(1-3): 499-525.
54. Hoog SS, Pawlowski JE, Alzari PM, Penning TM, Lewis M. Three-dimensional structure of rat liver 3 alpha-hydroxysteroid/dihydrodiol dehydrogenase: a member of the aldo-keto reductase superfamily. *Proc Natl Acad Sci U S A* 1994; **91**(7): 2517-21.

55. Jez JM, Flynn TG, Penning TM. A new nomenclature for the aldo-keto reductase superfamily. *Biochem Pharmacol* 1997; **54**(6): 639-47.
56. Zeng C-M, Chang L-L, Ying M-D, et al. Aldo-Keto Reductase AKR1C1-AKR1C4: Functions, Regulation, and Intervention for Anti-cancer Therapy. *Front Pharmacol* 2017; **8**: 119.
57. Jez JM, Bennett MJ, Schlegel BP, Lewis M, Penning TM. Comparative anatomy of the aldo-keto reductase superfamily. *Biochem J* 1997; **326 ( Pt 3)**(Pt 3): 625-36.
58. Chu X, He S, Liu Y, et al. Overview of human 20 alpha-hydroxysteroid dehydrogenase (AKR1C1): Functions, regulation, and structural insights of inhibitors. *Chem Biol Interact* 2022; **351**: 109746.
59. Huang F, Zheng Y, Li X, Luo H, Luo L. Ferroptosis-related gene AKR1C1 predicts the prognosis of non-small cell lung cancer. *Cancer Cell Int* 2021; **21**(1): 567.
60. Chang L-L, Lu P-H, Yang W, et al. AKR1C1 promotes non-small cell lung cancer proliferation via crosstalk between HIF-1α and metabolic reprogramming. *Transl Oncol* 2022; **20**: 101421.
61. Zhu H, Chang L-L, Yan F-J, et al. AKR1C1 Activates STAT3 to Promote the Metastasis of Non-Small Cell Lung Cancer. *Theranostics* 2018; **8**(3): 676-92.
62. Wei X, Wei Z, Li Y, Tan Z, Lin C. AKR1C1 Contributes to Cervical Cancer Progression via Regulating TWIST1 Expression. *Biochem Genet* 2021; **59**(2): 516-30.
63. Badmann S, Mayr D, Schmoeckel E, et al. AKR1C1/2 inhibition by MPA sensitizes platinum resistant ovarian cancer towards carboplatin. *Sci Rep* 2022; **12**(1): 1862.
64. Zhang Z, Qiu X, Yan Y, et al. Evaluation of Ferroptosis-related Gene AKR1C1 as a Novel Biomarker Associated with the Immune Microenvironment and Prognosis in Breast Cancer. *Int J Gen Med* 2021; **14**: 6189-200.
65. Rizner TL, Smuc T, Rupreht R, Sinkovec J, Penning TM. AKR1C1 and AKR1C3 may determine progesterone and estrogen ratios in endometrial cancer. *Mol Cell Endocrinol* 2006; **248**(1-2): 126-35.
66. Chang W-M, Chang Y-C, Yang Y-C, Lin S-K, Chang PM-H, Hsiao M. AKR1C1 controls cisplatin-resistance in head and neck squamous cell carcinoma through cross-talk with the STAT1/3 signaling pathway. *Journal of Experimental & Clinical Cancer Research : CR* 2019; **38**(1): 245.
67. Skarydova L, Nobilis M, Wsól V. Role of carbonyl reducing enzymes in the phase I biotransformation of the non-steroidal anti-inflammatory drug nabumetone in vitro. *Xenobiotica* 2013; **43**(4): 346-54.
68. Hu M, Sun D, Yu J, et al. Brusatol sensitizes endometrial hyperplasia and cancer to progestin by suppressing NRF2-TET1-AKR1C1-mediated progestin metabolism. *Lab Invest* 2022; **102**(12): 1335-45.
69. Zeng C, Zhu D, You J, et al. Liquiritin, as a Natural Inhibitor of AKR1C1, Could Interfere With the Progesterone Metabolism. *Front Physiol* 2019; **10**: 833.
70. Zhang A, Zhang J, Plymate S, Mostaghel EA. Classical and Non-Classical Roles for Pre-Receptor Control of DHT Metabolism in Prostate Cancer Progression. *Horm Cancer* 2016; **7**(2): 104-13.
71. Ji Q, Chang L, Stanczyk FZ, Ookhtens M, Sherrod A, Stolz A. Impaired dihydrotestosterone catabolism in human prostate cancer: critical role of AKR1C2 as a pre-receptor regulator of androgen receptor signaling. *Cancer Res* 2007; **67**(3): 1361-9.

72. Jin Y-X, Zhou X-F, Chen Y-Y, et al. Up-Regulated AKR1C2 is correlated with favorable prognosis in thyroid carcinoma. *J Cancer* 2019; **10**(15): 3543-52.
73. Zhang Z-F, Huang T-J, Zhang X-K, et al. AKR1C2 acts as a targetable oncogene in esophageal squamous cell carcinoma via activating PI3K/AKT signaling pathway. *J Cell Mol Med* 2020; **24**(17).
74. Johansson AGM, Nikamo P, Schalling M, Landén M. AKR1C4 gene variant associated with low euthymic serum progesterone and a history of mood irritability in males with bipolar disorder. *J Affect Disord* 2011; **133**(1-2): 346-51.
75. Shin S-Y, Fauman EB, Petersen A-K, et al. An atlas of genetic influences on human blood metabolites. *Nat Genet* 2014; **46**(6): 543-50.
76. Willer CJ, Schmidt EM, Sengupta S, et al. Discovery and refinement of loci associated with lipid levels. *Nat Genet* 2013; **45**(11): 1274-83.
77. Kelsey JL, Gammon MD, John EM. Reproductive factors and breast cancer. *Epidemiol Rev* 1993; **15**(1): 36-47.
78. Menarche, menopause, and breast cancer risk: individual participant meta-analysis, including 118 964 women with breast cancer from 117 epidemiological studies. *Lancet Oncol* 2012; **13**(11): 1141-51.
79. Li M, Lin J, Liang S, et al. The role of age at menarche and age at menopause in Alzheimer's disease: evidence from a bidirectional mendelian randomization study. *Aging (Albany NY)* 2021; **13**(15): 19722-49.
80. Lakshman R, Forouhi NG, Sharp SJ, et al. Early age at menarche associated with cardiovascular disease and mortality. *J Clin Endocrinol Metab* 2009; **94**(12): 4953-60.
81. Mishra SR, Chung HF, Waller M, Mishra GD. Duration of estrogen exposure during reproductive years, age at menarche and age at menopause, and risk of cardiovascular disease events, all-cause and cardiovascular mortality: a systematic review and meta-analysis. *BJOG* 2021; **128**(5): 809-21.
82. Ryu S, Chang Y, Choi Y, et al. Age at menarche and non-alcoholic fatty liver disease. *J Hepatol* 2015; **62**(5): 1164-70.
83. Guo S-S, Chen Y-Z, Liu L-T, et al. Prognostic significance of AKR1C4 and the advantage of combining EBV DNA to stratify patients at high risk of locoregional recurrence of nasopharyngeal carcinoma. *BMC Cancer* 2022; **22**(1): 880.
84. Miao Y, Li Q, Wang J, et al. Prognostic implications of metabolism-associated gene signatures in colorectal cancer. *PeerJ* 2020; **8**: e9847.
85. Suzuki-Yamamoto T, Nishizawa M, Fukui M, et al. cDNA cloning, expression and characterization of human prostaglandin F synthase. *FEBS Lett* 1999; **462**(3): 335-40.
86. Penning TM, Burczynski ME, Jez JM, et al. Human 3alpha-hydroxysteroid dehydrogenase isoforms (AKR1C1-AKR1C4) of the aldo-keto reductase superfamily: functional plasticity and tissue distribution reveals roles in the inactivation and formation of male and female sex hormones. *Biochem J* 2000; **351**(Pt 1): 67-77.
87. Zhou Q, Tian W, Jiang Z, et al. A Positive Feedback Loop of AKR1C3-Mediated Activation of NF-κB and STAT3 Facilitates Proliferation and Metastasis in Hepatocellular Carcinoma. *Cancer Res* 2021; **81**(5): 1361-74.
88. Wu C, Dai C, Li X, et al. AKR1C3-dependent lipid droplet formation confers hepatocellular carcinoma cell adaptability to targeted therapy. *Theranostics* 2022; **12**(18): 7681-98.
89. Liu Y, Chen Y, Jiang J, et al. Development of highly potent and specific

AKR1C3 inhibitors to restore the chemosensitivity of drug-resistant breast cancer. *Eur J Med Chem* 2023; **247**: 115013.
90. Yamashita N, Kanno Y, Saito N, et al. Aryl hydrocarbon receptor counteracts pharmacological efficacy of doxorubicin via enhanced AKR1C3 expression in triple negative breast cancer cells. *Biochem Biophys Res Commun* 2019; **516**(3): 693-8.
91. Hertzog JR, Zhang Z, Bignan G, et al. AKR1C3 mediates pan-AR antagonist resistance in castration-resistant prostate cancer. *Prostate* 2020; **80**(14): 1223-32.
92. Niu B, Liao K, Zhou Y, et al. Application of glutathione depletion in cancer therapy: Enhanced ROS-based therapy, ferroptosis, and chemotherapy. *Biomaterials* 2021; **277**: 121110.
93. Zhou C, Wang Z, Li J, et al. Aldo-Keto Reductase 1C3 Mediates Chemotherapy Resistance in Esophageal Adenocarcinoma via ROS Detoxification. *Cancers (Basel)* 2021; **13**(10).
94. Schaue D, McBride WH. Opportunities and challenges of radiotherapy for treating cancer. *Nat Rev Clin Oncol* 2015; **12**(9): 527-40.
95. Xie L, Yu J, Guo W, et al. Aldo-keto reductase 1C3 may be a new radioresistance marker in non-small-cell lung cancer. *Cancer Gene Ther* 2013; **20**(4): 260-6.
96. Sun S-Q, Gu X, Gao X-S, et al. Overexpression of AKR1C3 significantly enhances human prostate cancer cells resistance to radiation. *Oncotarget* 2016; **7**(30): 48050-8.
97. Xiong W, Zhao J, Yu H, et al. Elevated expression of AKR1C3 increases resistance of cancer cells to ionizing radiation via modulation of oxidative stress. *PLoS One* 2014; **9**(11): e111911.
98. Zimta A-A, Cenariu D, Irimie A, et al. The Role of Nrf2 Activity in Cancer Development and Progression. *Cancers (Basel)* 2019; **11**(11).
99. Xiong W, Hu XHW. AKR1C3 and β-catenin expression in non-small cell lung cancer and relationship with radiation resistance. *J BUON* 2021; **26**(3): 802-11.
100. Lorenzo-González M, Torres-Durán M, Barbosa-Lorenzo R, Provencio-Pulla M, Barros-Dios JM, Ruano-Ravina A. Radon exposure: a major cause of lung cancer. *Expert Rev Respir Med* 2019; **13**(9): 839-50.
101. Moon J, Yoo H. Residential radon exposure and leukemia: A meta-analysis and dose-response meta-analyses for ecological, case-control, and cohort studies. *Environ Res* 2021; **202**: 111714.
102. Loiselle JJ, Knee JM, Sutherland LC. Human lung epithelial cells cultured in the presence of radon-emitting rock experience gene expression changes similar to those associated with tobacco smoke exposure. *J Environ Radioact* 2019; **196**: 64-81.
103. Adeniji AO, Chen M, Penning TM. AKR1C3 as a target in castrate resistant prostate cancer. *J Steroid Biochem Mol Biol* 2013; **137**: 136-49.
104. Kafka M, Mayr F, Temml V, et al. Dual Inhibitory Action of a Novel AKR1C3 Inhibitor on Both Full-Length AR and the Variant AR-V7 in Enzalutamide Resistant Metastatic Castration Resistant Prostate Cancer. *Cancers (Basel)* 2020; **12**(8).
105. Yin YD, Fu M, Brooke DG, Heinrich DM, Denny WA, Jamieson SMF. The Activity of SN33638, an Inhibitor of AKR1C3, on Testosterone and 17β-Estradiol Production and Function in Castration-Resistant Prostate Cancer and ER-

Positive Breast Cancer. *Front Oncol* 2014; **4**: 159.
106. Li X, Hong X, Gao X, et al. Methyl jasmonate enhances the radiation sensitivity of esophageal carcinoma cells by inhibiting the 11-ketoprostaglandin reductase activity of AKR1C3. *Cancer Manag Res* 2018; **10**: 3149-58.
107. Jiao Y, Cao F, Liu H. Radiation-induced Cell Death and Its Mechanisms. *Health Phys* 2022; **123**(5): 376-86.
108. Dixon SJ, Lemberg KM, Lamprecht MR, et al. Ferroptosis: an iron-dependent form of nonapoptotic cell death. *Cell* 2012; **149**(5): 1060-72.
109. Xie Y, Hou W, Song X, et al. Ferroptosis: process and function. *Cell Death Differ* 2016; **23**(3): 369-79.
110. Mou Y, Wang J, Wu J, et al. Ferroptosis, a new form of cell death: opportunities and challenges in cancer. *J Hematol Oncol* 2019; **12**(1): 34.
111. Bersuker K, Hendricks JM, Li Z, et al. The CoQ oxidoreductase FSP1 acts parallel to GPX4 to inhibit ferroptosis. *Nature* 2019; **575**(7784): 688-92.
112. Imai H, Matsuoka M, Kumagai T, Sakamoto T, Koumura T. Lipid Peroxidation-Dependent Cell Death Regulated by GPx4 and Ferroptosis. *Curr Top Microbiol Immunol* 2017; **403**: 143-70.
113. Mao C, Liu X, Zhang Y, et al. DHODH-mediated ferroptosis defence is a targetable vulnerability in cancer. *Nature* 2021; **593**(7860): 586-90.
114. Chen X, Li J, Kang R, Klionsky DJ, Tang D. Ferroptosis: machinery and regulation. *Autophagy* 2021; **17**(9): 2054-81.
115. Ursini F, Maiorino M. Lipid peroxidation and ferroptosis: The role of GSH and GPx4. *Free Radic Biol Med* 2020; **152**: 175-85.
116. Hu K, Li K, Lv J, et al. Suppression of the SLC7A11/glutathione axis causes synthetic lethality in KRAS-mutant lung adenocarcinoma. *J Clin Invest* 2020; **130**(4): 1752-66.
117. Ye Y, Chen A, Li L, et al. Repression of the antiporter SLC7A11/glutathione/glutathione peroxidase 4 axis drives ferroptosis of vascular smooth muscle cells to facilitate vascular calcification. *Kidney Int* 2022; **102**(6): 1259-75.
118. Yuan Y, Zhai Y, Chen J, Xu X, Wang H. Kaempferol Ameliorates Oxygen-Glucose Deprivation/Reoxygenation-Induced Neuronal Ferroptosis by Activating Nrf2/SLC7A11/GPX4 Axis. *Biomolecules* 2021; **11**(7).
119. Li J, Cao F, Yin H-L, et al. Ferroptosis: past, present and future. *Cell Death Dis* 2020; **11**(2): 88.
120. Doll S, Freitas FP, Shah R, et al. FSP1 is a glutathione-independent ferroptosis suppressor. *Nature* 2019; **575**(7784): 693-8.
121. Vasan K, Werner M, Chandel NS. Mitochondrial Metabolism as a Target for Cancer Therapy. *Cell Metab* 2020; **32**(3): 341-52.
122. Hassannia B, Vandenabeele P, Vanden Berghe T. Targeting Ferroptosis to Iron Out Cancer. *Cancer Cell* 2019; **35**(6): 830-49.
123. Liang D, Minikes AM, Jiang X. Ferroptosis at the intersection of lipid metabolism and cellular signaling. *Mol Cell* 2022; **82**(12): 2215-27.
124. Ouyang S, Li H, Lou L, et al. Inhibition of STAT3-ferroptosis negative regulatory axis suppresses tumor growth and alleviates chemoresistance in gastric cancer. *Redox Biol* 2022; **52**: 102317.
125. Wang Y, Zheng L, Shang W, et al. Wnt/beta-catenin signaling confers ferroptosis resistance by targeting GPX4 in gastric cancer. *Cell Death Differ* 2022; **29**(11): 2190-202.
126. Liu M-Y, Li H-M, Wang X-Y, et al. TIGAR drives colorectal cancer

ferroptosis resistance through ROS/AMPK/SCD1 pathway. *Free Radic Biol Med* 2022; **182**: 219-31.
127. Ebrahimi N, Adelian S, Shakerian S, et al. Crosstalk between ferroptosis and the epithelial-mesenchymal transition: Implications for inflammation and cancer therapy. *Cytokine Growth Factor Rev* 2022; **64**: 33-45.
128. Wang H, Huang Q, Xia J, et al. The E3 Ligase MIB1 Promotes Proteasomal Degradation of NRF2 and Sensitizes Lung Cancer Cells to Ferroptosis. *Mol Cancer Res* 2022; **20**(2): 253-64.
129. Fang K, Du S, Shen D, et al. SUFU suppresses ferroptosis sensitivity in breast cancer cells via Hippo/YAP pathway. *iScience* 2022; **25**(7): 104618.
130. Dixon SJ. Ferroptosis: bug or feature? *Immunol Rev* 2017; **277**(1): 150-7.
131. Wang S-J, Gu W. To be, or not to be: functional dilemma of p53 metabolic regulation. *Curr Opin Oncol* 2014; **26**(1): 78-85.
132. Jiang L, Kon N, Li T, et al. Ferroptosis as a p53-mediated activity during tumour suppression. *Nature* 2015; **520**(7545): 57-62.
133. Tarangelo A, Magtanong L, Bieging-Rolett KT, et al. p53 Suppresses Metabolic Stress-Induced Ferroptosis in Cancer Cells. *Cell Rep* 2018; **22**(3): 569-75.
134. Lei G, Zhuang L, Gan B. Targeting ferroptosis as a vulnerability in cancer. *Nat Rev Cancer* 2022; **22**(7): 381-96.
135. Liang C, Zhang X, Yang M, Dong X. Recent Progress in Ferroptosis Inducers for Cancer Therapy. *Adv Mater* 2019; **31**(51): e1904197.
136. Chen H, Zhang W, Zhu G, Xie J, Chen X. Rethinking cancer nanotheranostics. *Nat Rev Mater* 2017; **2**.
137. Zhao L, Zhou X, Xie F, et al. Ferroptosis in cancer and cancer immunotherapy. *Cancer Commun (Lond)* 2022; **42**(2).
138. Li H, Yang P, Wang J, et al. HLF regulates ferroptosis, development and chemoresistance of triple-negative breast cancer by activating tumor cell-macrophage crosstalk. *J Hematol Oncol* 2022; **15**(1): 2.
139. Koppula P, Lei G, Zhang Y, et al. A targetable CoQ-FSP1 axis drives ferroptosis- and radiation-resistance in KEAP1 inactive lung cancers. *Nat Commun* 2022; **13**(1): 2206.
140. Delaney G, Jacob S, Featherstone C, Barton M. The role of radiotherapy in cancer treatment: estimating optimal utilization from a review of evidence-based clinical guidelines. *Cancer* 2005; **104**(6): 1129-37.
141. Azzam EI, Jay-Gerin J-P, Pain D. Ionizing radiation-induced metabolic oxidative stress and prolonged cell injury. *Cancer Lett* 2012; **327**(1-2): 48-60.
142. Lei G, Zhang Y, Koppula P, et al. The role of ferroptosis in ionizing radiation-induced cell death and tumor suppression. *Cell Res* 2020; **30**(2): 146-62.
143. Zhang W, Sun Y, Bai L, et al. RBMS1 regulates lung cancer ferroptosis through translational control of SLC7A11. *J Clin Invest* 2021; **131**(22).
144. Loira-Pastoriza C, Todoroff J, Vanbever R. Delivery strategies for sustained drug release in the lungs. *Adv Drug Deliv Rev* 2014; **75**: 81-91.
145. Li Y, Yang J, Gu G, et al. Pulmonary Delivery of Theranostic Nanoclusters for Lung Cancer Ferroptosis with Enhanced Chemodynamic/Radiation Synergistic Therapy. *Nano Lett* 2022; **22**(3): 963-72.
146. Feng L, Zhao K, Sun L, et al. SLC7A11 regulated by NRF2 modulates esophageal squamous cell carcinoma radiosensitivity by inhibiting ferroptosis. *J Transl Med* 2021; **19**(1): 367.

147. Luo H, Wang X, Song S, Wang Y, Dan Q, Ge H. Targeting stearoyl-coa desaturase enhances radiation induced ferroptosis and immunogenic cell death in esophageal squamous cell carcinoma. *Oncoimmunology* 2022; **11**(1): 2101769.
148. Jiang K, Yin X, Zhang Q, et al. STC2 activates PRMT5 to induce radioresistance through DNA damage repair and ferroptosis pathways in esophageal squamous cell carcinoma. *Redox Biol* 2023; **60**: 102626.
149. Singh NP, McCoy MT, Tice RR, Schneider EL. A simple technique for quantitation of low levels of DNA damage in individual cells. *Exp Cell Res* 1988; **175**(1): 184-91.
150. Mah LJ, El-Osta A, Karagiannis TC. gammaH2AX: a sensitive molecular marker of DNA damage and repair. *Leukemia* 2010; **24**(4): 679-86.
151. Raavi V, Perumal V, F D Paul S. Potential application of γ-H2AX as a biodosimetry tool for radiation triage. *Mutat Res Rev Mutat Res* 2021; **787**: 108350.
152. Liu Y, Li H, Wilson CN, Bai HJ, Boufraqech M, Weyemi U. Histone H2AX promotes metastatic progression by preserving glycolysis via hexokinase-2. *Sci Rep* 2022; **12**(1): 3758.
153. Miotto G, Rossetto M, Di Paolo ML, et al. Insight into the mechanism of ferroptosis inhibition by ferrostatin-1. *Redox Biol* 2020; **28**: 101328.
154. Carraro A, Trevellin E, Fassan M, et al. Esophageal adenocarcinoma microenvironment: Peritumoral adipose tissue effects associated with chemoresistance. *Cancer Sci* 2017; **108**(12): 2393-404.
155. Buckley AM, Dunne MR, Lynam-Lennon N, et al. Pyrazinib (P3), [(E)-2-(2-Pyrazin-2-yl-vinyl)-phenol], a small molecule pyrazine compound enhances radiosensitivity in oesophageal adenocarcinoma. *Cancer Lett* 2019; **447**: 115-29.
156. Xiong W, Huang X, Yao S, Wang L, Wang J, Wang X. Expression of AKR1C3, β-Catenin and LEF1 in Esophageal Squamous Cell Carcinoma and the Relationship with Radiation Resistance. *Iran J Public Health* 2021; **50**(7): 1488-90.
157. Liu H, Gao L, Xie T, Li J, Zhai T-S, Xu Y. Identification and Validation of a Prognostic Signature for Prostate Cancer Based on Ferroptosis-Related Genes. *Front Oncol* 2021; **11**: 623313.
158. Wang Y, Yang J, Chen S, Wang W, Teng L. Identification and Validation of a Prognostic Signature for Thyroid Cancer Based on Ferroptosis-Related Genes. *Genes (Basel)* 2022; **13**(6).
159. Yin H, Lin M, Liang S, et al. Ferroptosis-related gene signature predicts prognosis in kidney renal papillary cell carcinoma. *Front Oncol* 2022; **12**: 988867.
160. Pan B, Li Y, Xu Z, et al. Identifying a novel ferroptosis-related prognostic score for predicting prognosis in chronic lymphocytic leukemia. *Front Immunol* 2022; **13**: 962000.
161. Miao Y-D, Kou Z-Y, Wang J-T, Mi D-H. Prognostic implications of ferroptosis-associated gene signature in colon adenocarcinoma. *World J Clin Cases* 2021; **9**(29): 8671-93.
162. Dai T, Li J, Lu X, et al. Prognostic Role and Potential Mechanisms of the Ferroptosis-Related Metabolic Gene Signature in Hepatocellular Carcinoma. *Pharmgenomics Pers Med* 2021; **14**: 927-45.
163. Chen J, Zhang J, Tian W, et al. AKR1C3 suppresses ferroptosis in hepatocellular carcinoma through regulation of YAP/SLC7A11 signaling pathway. *Mol Carcinog* 2023.
164. Srinivas US, Tan BWQ, Vellayappan BA, Jeyasekharan AD. ROS and the

DNA damage response in cancer. *Redox Biol* 2019; **25**: 101084.
165. Drummen GPC, van Liebergen LCM, Op den Kamp JAF, Post JA. C11-BODIPY(581/591), an oxidation-sensitive fluorescent lipid peroxidation probe: (micro)spectroscopic characterization and validation of methodology. *Free Radic Biol Med* 2002; **33**(4): 473-90.
166. Zhao Y, Li Y, Zhang R, Wang F, Wang T, Jiao Y. The Role of Erastin in Ferroptosis and Its Prospects in Cancer Therapy. *Onco Targets Ther* 2020; **13**: 5429-41.
167. Forcina GC, Dixon SJ. GPX4 at the Crossroads of Lipid Homeostasis and Ferroptosis. *Proteomics* 2019; **19**(18): e1800311.
168. Tang Z, Li C, Kang B, Gao G, Li C, Zhang Z. GEPIA: a web server for cancer and normal gene expression profiling and interactive analyses. *Nucleic Acids Res* 2017; **45**(W1).
169. Chen Q, Zheng W, Guan J, et al. SOCS2-enhanced ubiquitination of SLC7A11 promotes ferroptosis and radiosensitization in hepatocellular carcinoma. *Cell Death Differ* 2023; **30**(1): 137-51.
170. Liu R, Liu L, Bian Y, et al. The Dual Regulation Effects of ESR1/NEDD4L on SLC7A11 in Breast Cancer Under Ionizing Radiation. *Front Cell Dev Biol* 2021; **9**: 772380.
171. Jiang L, Kon N, Li T, et al. Ferroptosis as a p53-mediated activity during tumour suppression. *Nature* 2015; **520**(7545): 57-62.
172. Chu B, Kon N, Chen D, et al. ALOX12 is required for p53-mediated tumour suppression through a distinct ferroptosis pathway. *Nat Cell Biol* 2019; **21**(5): 579-91.
173. Wang Z, Zhang X, Tian X, et al. CREB stimulates GPX4 transcription to inhibit ferroptosis in lung adenocarcinoma. *Oncol Rep* 2021; **45**(6).
174. Degirmenci U, Wang M, Hu J. Targeting Aberrant RAS/RAF/MEK/ERK Signaling for Cancer Therapy. *Cells* 2020; **9**(1).
175. Simamura E, Shimada H, Hatta T, Hirai K-I. Mitochondrial voltage-dependent anion channels (VDACs) as novel pharmacological targets for anti-cancer agents. *J Bioenerg Biomembr* 2008; **40**(3): 213-7.
176. Yagoda N, von Rechenberg M, Zaganjor E, et al. RAS-RAF-MEK-dependent oxidative cell death involving voltage-dependent anion channels. *Nature* 2007; **447**(7146): 864-8.
177. Dixon SJ, Patel DN, Welsch M, et al. Pharmacological inhibition of cystine-glutamate exchange induces endoplasmic reticulum stress and ferroptosis. *Elife* 2014; **3**: e02523.
178. Zheng X, Wang Q, Zhou Y, et al. N-acetyltransferase 10 promotes colon cancer progression by inhibiting ferroptosis through N4-acetylation and stabilization of ferroptosis suppressor protein 1 (FSP1) mRNA. *Cancer Commun (Lond)* 2022; **42**(12): 1347-66.
179. Yuan J, Lv T, Yang J, et al. HDLBP-stabilized lncFAL inhibits ferroptosis vulnerability by diminishing Trim69-dependent FSP1 degradation in hepatocellular carcinoma. *Redox Biol* 2022; **58**: 102546.
180. Peraldo-Neia C, Ostano P, Mello-Grand M, et al. AKR1C3 is a biomarker and druggable target for oropharyngeal tumors. *Cell Oncol (Dordr)* 2021; **44**(2): 357-72.
181. Reddi D, Seaton BW, Woolston D, et al. AKR1C3 expression in T acute lymphoblastic leukemia/lymphoma for clinical use as a biomarker. *Sci Rep* 2022; **12**(1): 5809.

182. Moradi Manesh D, El-Hoss J, Evans K, et al. AKR1C3 is a biomarker of sensitivity to PR-104 in preclinical models of T-cell acute lymphoblastic leukemia. *Blood* 2015; **126**(10): 1193-202.
183. Tian Y, Zhao L, Zhang H, et al. AKR1C3 overexpression may serve as a promising biomarker for prostate cancer progression. *Diagn Pathol* 2014; **9**: 42.